



Non-orthogonal Failure Behavior of Roadway Surrounding Rock Subjected to Deep Complicated Stress

Zongyu Ma¹ · Jianping Zuo^{1,2} · Fan Zhu¹ · Haiyan Liu¹ · Chengyi Xu¹

Received: 28 February 2023 / Accepted: 17 May 2023 / Published online: 3 June 2023
© The Author(s), under exclusive licence to Springer-Verlag GmbH Austria, part of Springer Nature 2023

Abstract

Based on the characteristics of real stress distribution in coal mining, the evolution law of plastic zone shape and spatial position were investigated. The stress model of roadway with non-orthogonal state of in-situ stress and mining-induced stress was constructed. The boundary equation of the roadway plastic zone under in-situ stress deflection was deduced. Additionally, the evolution mechanism of the roadway plastic zone was analysed. We found that the shape and spatial position of the roadway plastic zone are jointly determined by in-situ stress deflection angle α , mining-induced stress concentration coefficient K , and equivalent lateral pressure coefficient η' when the mechanical parameters (rock cohesion c ; internal friction angle φ) were fixed. Specifically, the plastic zone experiences the cyclic evolution phenomenon, where the plastic zone shape varies from petal–ellipse–circle–ellipse–petal shapes in morphology. In this study, we expound the general evolution law of roadway plastic zone under different geological, working conditions and mechanical parameters. The main controlling factors and mechanism of the shape and spatial position evolution of the plastic zone are revealed. A numerical model was established to study the evolution law of plastic zone during the change of corresponding parameters. The results show that the traditional method of predicting the shape of plastic zone by lateral pressure coefficient is inaccurate. The plastic zone distribution calculated using this method was compared with the roadway deformation measured in 1305 bottom drainage roadway of Hudi mine, and the comparison results were in good accordance. The results of this study have certain universality, and enrich the understanding of the roadway plastic zone. It can provide theoretical reference for roadway excavation and support design under different geological and in-situ stress conditions.

Highlights

- The non-orthogonal failure behavior of the roadway with the change of complicated stress state is revealed.
- Plastic zone experiences the cyclic evolution phenomenon, where the plastic zone shape varies from petal-ellipse-circle-ellipse-petal shapes in morphology.
- Main controlling factors and mechanism of the shape and spatial position evolution of the plastic zone are summarized.
- The unsymmetrical failure mechanism of roadway under non-orthogonal stress state is revealed.

Keywords In-situ stress direction · Mining-induced stress · Non-orthogonal stress · Plastic zone of surrounding rock · Failure characteristics

✉ Jianping Zuo
zjp@cumtb.edu.cn

¹ School of Mechanics and Civil Engineering, China University of Mining and Technology (Beijing), Beijing 100083, China

² State Key Laboratory of Coal Resources and Safe Mining, China University of Mining and Technology, Beijing 100083, China

1 Introduction

Coal resources occupy an important position in the world energy system (Aydin 2015; Aydin et al. 2015). The proportion of coal in primary energy consumption has always been at a high level due to its rich reserves (Zuo et al. 2021). Global coal consumption grew over 6% in 2021 (Zhang et al. 2023; Feng et al. 2020). China accounted for over 70% of the growth

in coal demand (BP 2022). Shallow coal resources are gradually depleted. The depth of coal mining is gradually increasing. The complex stress environment in deep areas can seriously affect the stability of roadway.

The deep rock mass often shows the characteristics of uneven distribution of stress and high stress level compared with the shallow rock mass. Therefore, the roadway excavated in the deep rock mass often has continuous large deformation, collapse, and other disaster phenomena. Solving this kind of disaster problem using conventional support methods is difficult (Fujii et al. 2011; Piotr et al. 2017; Zuo et al. 2019; Mo et al. 2020). Existing studies have shown that (Jiang et al. 2017; Sun et al. 2021; Yu et al. 2022), the essence of deformation and failure of surrounding rock is that excavation disturbance breaks the original stress balance of deep rock mass, resulting in sudden unloading of local rock mass. Moreover, the disturbance stress (or mining stress) caused by excavation acts on the rock mass, causing a sharp increase in the differential stress of rock mass, there by forming a plastic zone within a certain range of excavation area. However, the deep stress state is complex and difficult to analyse, which is the main factor restricting the in-depth study of roadway surrounding rock deformation and failure. Presently, there are many assumptions in the research of deep rock mass, in which the stress state is generally assumed to be an orthogonal stress state, i.e., the stress distribution is perpendicular to each other. Thus, based on elastic or plastic theory and yield criterion, the approximate range of roadway failure can be obtained. However, this treatment method cannot truly reflect the influence mechanism of various stresses in deep areas on surrounding rock failure of roadway. The real stress state in deep areas is not orthogonal. Generally, in-situ stress and mining stress are non-orthogonal stress states. Therefore, it is essential to conduct research on the failure characteristics of roadway surrounding rock under the non-orthogonal state of in-situ stress and mining-induced stress, and to explore the action mechanism of the angle between in-situ stress and mining-induced stress on roadway failure. Restoring the real stress situation of deep roadway and guide the support of deep roadway has great theoretical and practical significance.

Numerous achievements have been made in the research on the failure mechanism of roadway surrounding rock under the condition of orthogonal stress. As early as 1938, Fenner proposed the calculation theory of the roadway plastic zone under the condition of orthogonal stress, and proposed the original Fenner formula (Fenner 1938). Subsequently, Caquot considered the gravity effect of rock mass in the plastic zone, and established the Caquot formula (Caquot 1940). Talobre revised Fenner formula in 1960 to form Fenner-Talobre formula (also known as the modified Fenner formula), which was used until now (Talobre 1960; Kastner 1962; Roussev 1998; Xu and Yu 2006). In the following

decades, based on the above mentioned theory and by considering different strength theories, many scholars deduced additional formulas for circular tunnels in uniform medium and obtained the corresponding elastic–plastic solutions. These works expanded and improved the mentioned theory (Brown et al. 1983; Papanastasiou and Durban 1997). Recently, a stress model of roadway surrounding rock based on Fenner formula, Kastner formula and elastic–plastic theory was gradually developed, which is extensively used in the study of roadway roof fall mechanism, rock burst prevention, roadway water inrush mechanism, large deformation of surrounding rock, etc. (Guo et al. 2019, 2021; Fan et al. 2020).

Many scholars have conducted numerous studies on mining-induced stress caused by coal mining. Kodama et al. (2013) estimated the mining regional stress state by back analysis of mining-induced deformation. Li et al. (2018) introduced the mining-induced stress fields generated by different mining layouts. The spatial distribution of stress field of three typical underground mining methods of coal mine was studied by numerical simulation, and the change in stress concentration coefficient in front of the working face was analysed. Singh et al. (2011) briefly reviewed various research results on the development of mining stress, and discussed the field research results of mining stress development during depillaring under different geological mining conditions. Rezaei et al. (2015) developed an analytical model based on the strain energy balance in longwall coal mining to determine mining-induced stress over gates and pillars. The height of the distressed zone above the mined panel, total induced stress, abutment angle and coefficient of stress concentration over gates and pillars were determined analytically. Further summarizing the research status, highlighting the research content and main contributions of researchers. The specific content is shown in Table 1.

Based on the orthogonal stress state, the failure mechanism of roadway surrounding rock and the development characteristics of plastic zone were analysed systematically. However, in practical engineering, the stress condition of the roadway is a comprehensive superposition state of isotropic stress, which mainly includes two parts: in situ stress and mining-induced stress. Generally, the direction of in-situ stress is considered to be horizontal and vertical. However, due to the influence of faults, folds, structures, earthquakes, etc., the direction of in-situ stress will deflect (Yamamoto 2009; Yu et al. 2015a, b; Lucianetti et al. 2017; Mousavipour et al. 2020; Herrera et al. 2021; Lin and Zou 2021; Song et al. 2021). Mining-induced stress acts vertically on the heading face, but the in-situ stress and mining-induced stress are not orthogonal to each other. In other words, the roadway is usually in a non-orthogonal stress environment. It is not in line with the real stress environment to simply treat the anisotropic stress as an orthogonal state. Nevertheless, there are few studies on the non-orthogonal stress state

Table 1 Summary of current research on the failure mechanism of roadway and the distribution of mining-induced stress

Research area	Researcher (year)	Research contents	Main contributions
Failure mechanism of roadway	Fenner (1938)	Proposed the calculation theory of the roadway plastic zone; the Fenner formula was formed	The earliest method for calculating the plastic zone. It has been used up to now
	Caquot (1940)	Established Caquot formula considering the gravity effect of plastic zone rock mass	Caquot formula was frequently used in the following decades
	Talobre (1960) Kastner (1962)	Modified Fenner formula	The modified Finna formula is widely used in underground engineering
	Brown et al. (1983)	Introduced the calculation method of response curve for circular cross-section roadway excavation in rock mass	Improved understanding of the interaction between rocks and support structures
	Papanastasiou and Durban (1997)	A large-strain elastoplastic analysis was presented for a cylindrical cavity embedded in an infinite medium under uniform radial pressure	The established model can be used in the geotechnical, mining, and petroleum industries
	Guo et al. (2019, 2021) Fan et al. (2020)	Butterfly-shaped plastic zone theory	It can be used in roof fall mechanism, rock burst prevention and roadway water inrush mechanism
	Kodama et al. (2013)	Proposed a method to evaluate regional stress state and Young's modulus by analyzing the mining-induced deformation of ground	The effect of changes in regional strain state due to tectonic plate motion can be accounted
	Li et al. (2018)	The stress field distribution of non-pillar mining (NM), top-coal caving mining (TCM), and protective coal-seam mining (PCM) was studied	Provided stress distribution forms for different mining methods
	Singh et al. (2011)	The field research results of mining stress development was discussed	It is possible to estimate the influence range and value of the final mining-induced stress on the coal pillar
	Rezaei et al. (2015)	Developed an analytical model based on the strain energy balance in longwall coal mining to determine the mining-induced stress over gates and pillars	The proposed analytical model can be used to calculate the mining-induced stress

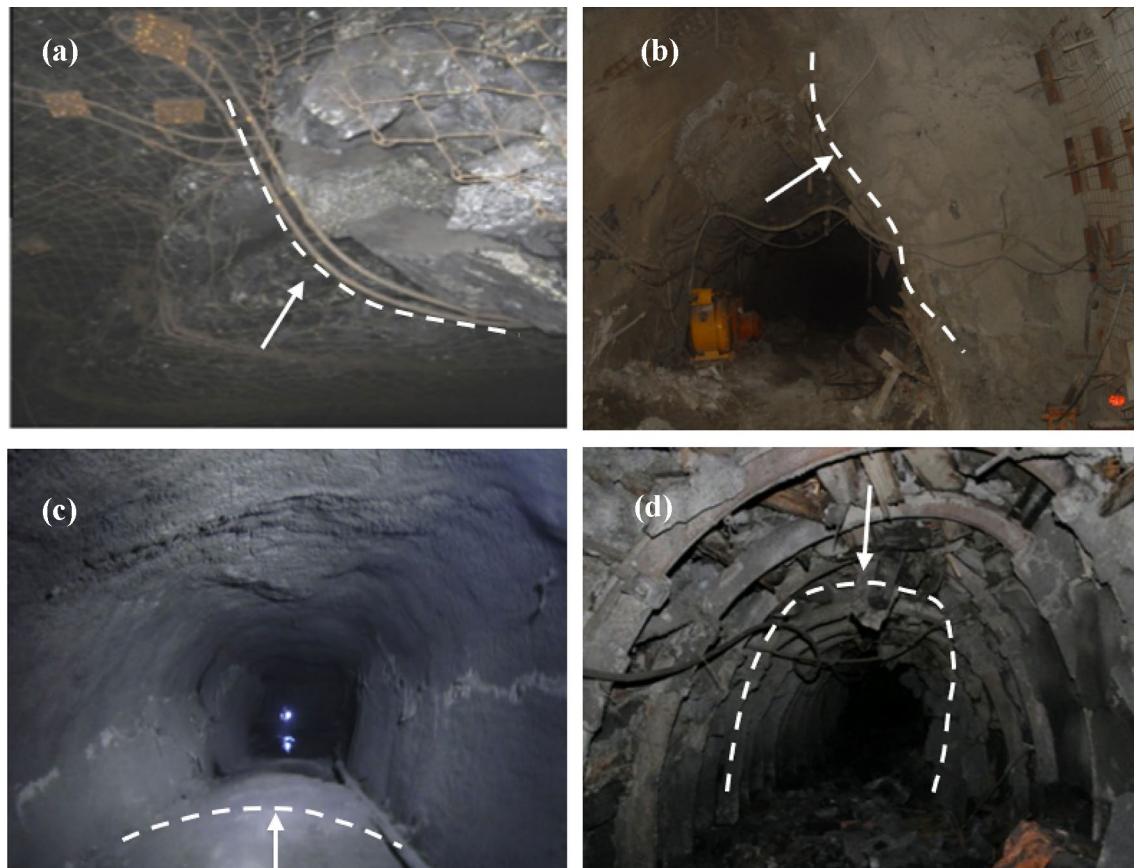


Fig. 1 Different failure modes of the roadway: **a** Roof falling (Tunlan Mine, Shanxi Province. Yu et al. 2015a, **b**) Rib spalling (Xin'an Mine, Gansu Province. Yang et al. 2017) **c** Floor heave (Jinchuan

Mine, Gansu Province. Li et al. 2020) **d** Unsymmetrical deformation (Xing'an Mine, Heilongjiang Province. Wang et al. 2019)

in line with the real stress environment. Therefore, the failure characteristics of roadway surrounding rock in non-orthogonal state of in-situ stress and mining-induced stress were analysed extensively in this study. Additionally, the existing theoretical calculation model of the plastic zone was improved. The morphological evolution process of the roadway plastic zone in the non-orthogonal state of in-situ stress and mining-induced stress was further studied. The action mechanism of the angle between in-situ stress and mining-induced stress on the development of the roadway plastic zone was revealed. The correctness of the theoretical calculation results is verified by numerical simulation and engineering examples. The research results can be used in roadway engineering designs.

2 Methods: Failure Modes and Mechanical Model of Roadways

The roadway failure mode in different mining areas is different. Moreover, the failure of different roadways in the same mining area is not similar. The failure modes of the roadway mainly include: roof falling, rib spalling, floor heaving and

unsymmetrical deformation, as shown in Fig. 1. These failures are mainly due to the different stress environments of the roadway.

The corresponding stress of each failure mode of the roadway is shown in Fig. 2. The stress condition of the roadway is jointly determined by the occurrence state of in-situ stress and excavation or mining-induced stress. The in-situ stress field in different areas is different, and the mining-induced stress is different in different excavation or mining methods. Therefore, the failure mode of roadway is also different. This indicates that in-situ stress and mining-induced stress are the main causes of roadway failure.

The direction of in-situ stress affects the stress state of surrounding rock near the roadway, resulting in different forms of deformation and failure of deep underground engineering. The mining-induced stress acts vertically on the working face, resulting in the plastic failure. This has a great impact on the plastic zone shape of the roadway surrounding rock. The roadway is in the in-situ stress field and mining-induced stress field, the distribution state and direction of its plastic zone are jointly controlled by the magnitude and direction of the stress around the roadway.

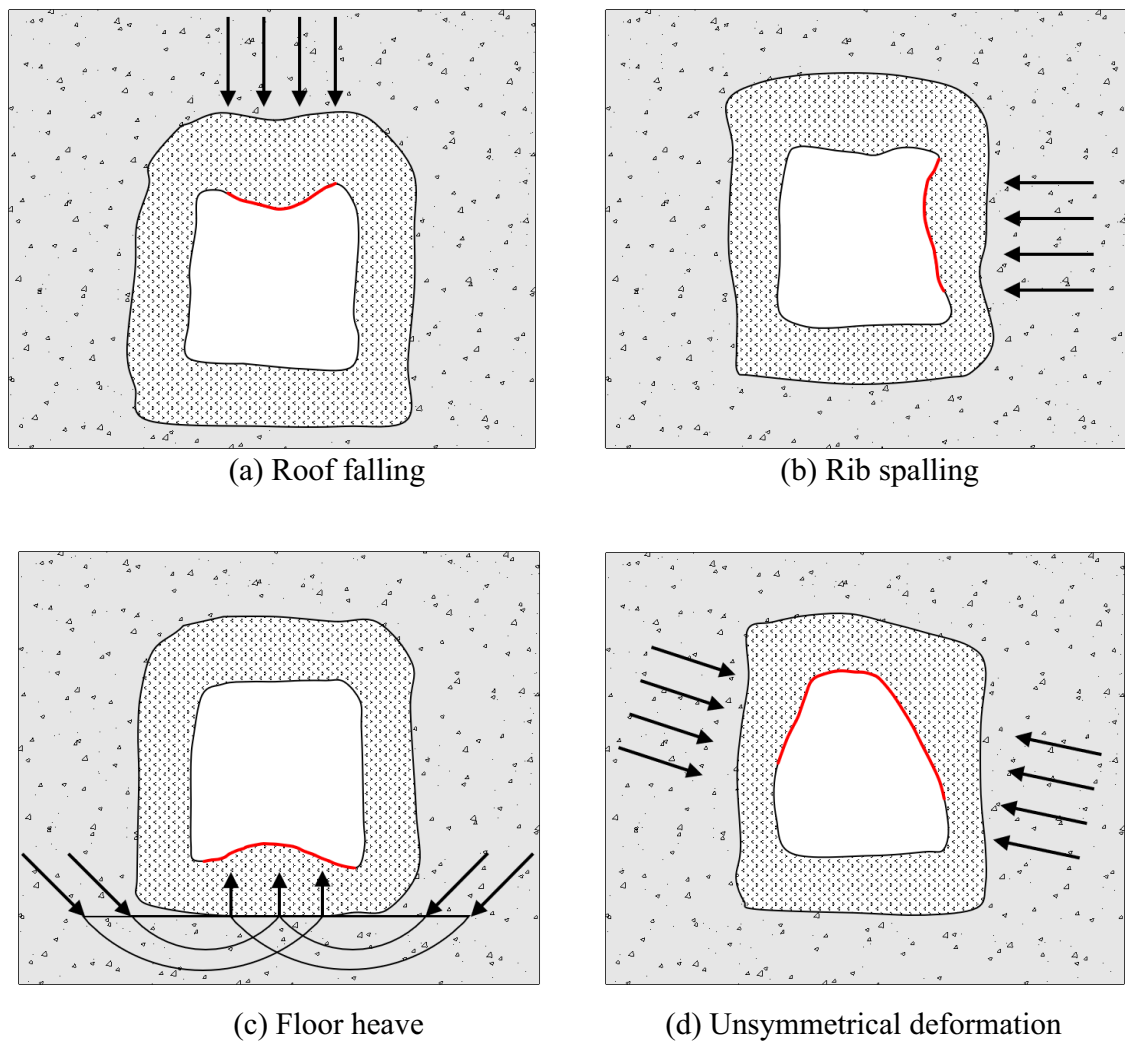


Fig. 2 Stress state of different failure modes

Considering the two factors of mining-induced stress and in-situ stress deflection, the range distribution and morphological characteristics of the roadway plastic zone were studied. The non-orthogonal angle α (deflection angle of in-situ stress) was introduced by considering the non-orthogonal state of in-situ stress and mining-induced stress. The mechanical model of roadway surrounding rock under the influence of mining-induced stress and in-situ stress deflection was established as shown in Fig. 3a, where, a is the roadway radius, r is the plastic zone radius, and $\sigma_1 \sigma_3$ are the maximum in-situ stress and minimum in-situ stress, respectively. $\eta = \sigma_1 / \sigma_3$ is the lateral pressure coefficient. Mining-induced stress σ' acts vertically on the roadway roof, and its direction is vertical and downward.

Once excavation is complete, an abutment pressure zone will be formed in front of the heading face. The stress increase range of the abutment pressure zone can be 3–5 times the

vertical in-situ stress (i.e., stress concentration coefficient K is 3–5) (Brown and Hudyma 2017; Kodama et al. 2013; Zhou et al. 2020). Therefore, the influence of mining-induced stress on the distribution of plastic zone of surrounding rock should be fully considered based on the existing model. When mining-induced stress exists, the mining-induced stress is equivalently decomposed in the direction of in-situ stress through mechanical decomposition, as shown in Fig. 3b. σ'_1 and σ'_3 are the equivalent stress after superposition of mining-induced stress. According to the principle of mechanics:

$$\sigma'_1 = \sigma_1 + \sigma' \sin \alpha \tag{1}$$

$$\sigma'_3 = \sigma_3 + \sigma' \cos \alpha \tag{2}$$

η' is defined as the equivalent lateral pressure coefficient, i.e., the ratio of equivalent stress:

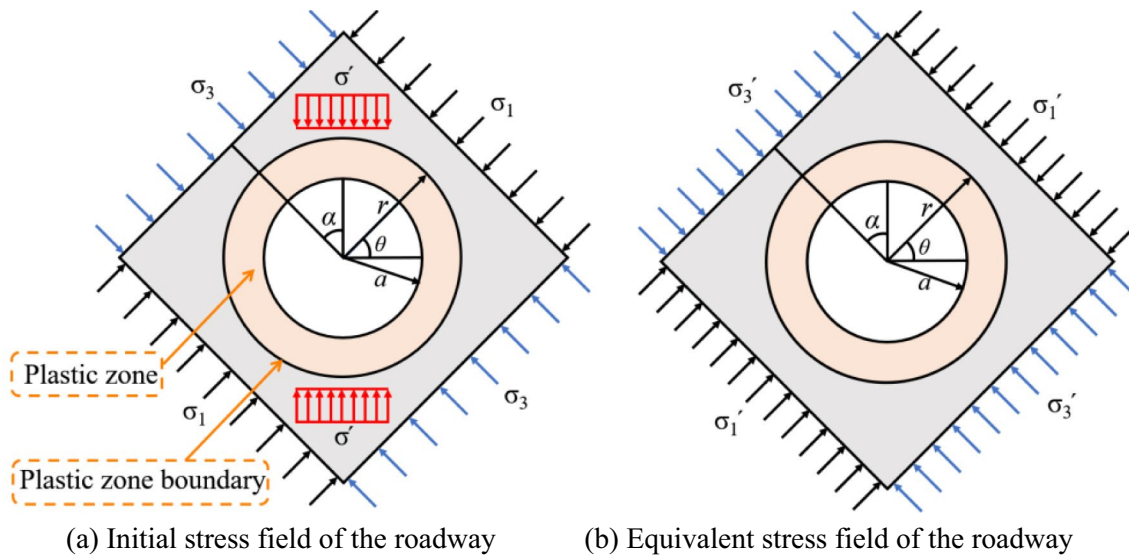


Fig. 3 Stress analysis model of the roadway

$$\eta' = \frac{\sigma_1'}{\sigma_3'} = \frac{\sigma_1 + \sigma' \sin \alpha}{\sigma_3 + \sigma' \cos \alpha} \quad (3)$$

Kastner (1962) modified the Fenner formula to form the Kastner formula. It can be used to solve the radius of the plastic zone. The Kastner formula without considering support pressure can be expressed as:

$$R = a \left[\frac{(p + c \cot \varphi)(1 - \sin \varphi)}{c \cot \varphi} \right]^{\frac{1 - \sin \varphi}{2 \sin \varphi}} \quad (4)$$

where: R represents the radius of the plastic zone, c is the cohesion of rock, φ is the internal friction angle, p represents the surrounding rock pressure under bidirectional isobaric conditions.

The applicable conditions of Kastner formula are: (1) The surrounding rock is an ideal elastoplastic material; (2) The in-situ stress is isotropic; (3) The failure criterion is Mohr–Coulomb criterion; (4) The roadway stress is a plane strain model, the intermediate principal stress σ_2 is not considered.

In addition, the following assumptions are made: (5) The rock mass is homogeneous and does not have layered features; (6) There are no faults, no water inrush, and no dip angle in the coal seam.

Combined with the Kastner formula, the radius of the plastic zone under biaxial unequal pressure conditions can be obtained (Guo et al. 2019). The mechanical model established in this study was analysed. The implicit equation of the distance between the plastic zone boundary and the roadway centre r in any direction when the in-situ stress deflects an angle α under the action of mining-induced stress σ' is obtained as follows:

$$\begin{aligned} & 9(1 - \eta')^2 \left(\frac{a}{r}\right)^8 + \left[-12(1 - \eta')^2 + 6(1 - \eta'^2) \cos 2(\theta - \alpha)\right] \left(\frac{a}{r}\right)^6 \\ & + \left[10(1 - \eta')^2 \cos^2 2(\theta - \alpha) - 4(1 - \eta')^2 \sin^2 \varphi \cos^2 2(\theta - \alpha) \right. \\ & \left. - 2(1 - \eta')^2 \sin^2 2(\theta - \alpha) - 4(1 - \eta'^2) \cos 2(\theta - \alpha) + (1 + \eta')^2\right] \left(\frac{a}{r}\right)^4 \\ & + \left[-4(1 - \eta')^2 \cos 4(\theta - \alpha) + 2(1 - \eta'^2) \cos 2(\theta - \alpha) \right. \\ & \left. - 4(1 - \eta'^2) \sin^2 \varphi \cos 2(\theta - \alpha) - \frac{4c(1 - \eta') \sin 2\varphi \cos 2(\theta - \alpha)}{\sigma_3'}\right] \left(\frac{a}{r}\right)^2 \\ & + \left[(1 - \eta')^2 - \sin^2 \varphi \left(1 + \eta' + \frac{2c \cos \varphi}{\sigma_3' \sin \varphi}\right)^2\right] = 0 \end{aligned} \quad (5)$$

where r is the radius of the plastic zone in the direction of θ .

3 Results: Non-orthogonal Failure Behaviors Subjected to Different Stress State

3.1 Influence of In-Situ Stress on the Plastic Zone

Deep roadway has the characteristics of high in-situ stress. The vertical in-situ stress caused by gravity usually exceeds the compressive strength of engineering rock mass (> 20 MPa). The stress concentration level caused by engineering excavation is significantly greater than the strength of engineering rock mass (> 40 MPa). There is tectonic stress field and residual tectonic stress field. The superposition and accumulation of the two stress fields leads to a high stress state. In this section, the magnitude of in-situ stress is determined according to the measured data of Chinese mainland. Considering the buried depth as the medium, the in-situ stress under different buried depths of kilometre level roadway is calculated, which is used as the basis for parameter selection.

Kang et al. (2010) organized the in-situ stress test data of 883 coal mines in various regions of China. Here, the data in a statistical sense are used. It reflects the characteristics of the in-situ stress assignment in China Mainland. The fitting relationship between the magnitude of in-situ stress and buried depth in China was obtained:

$$\begin{cases} \sigma_v = 0.0245H \\ \sigma_H = 0.021H + 3.267 \\ \sigma_h = 0.011H + 1.954 \end{cases} \quad (6)$$

where, H is the buried depth, and σ_v , σ_H , and σ_h represent the vertical in-situ stress, maximum horizontal in-situ stress, and minimum horizontal in-situ stress, respectively.

According to Eq. (6), the vertical stress increases approximately by 2.5 MPa for every 100 m increase in buried depth. Therefore, the vertical stress of kilometre deep roadway can reach approximately 25 MPa. However, in the regional stress field near the roadway, owing to excavation and mining, the regional maximum principal stress is not equal to the maximum horizontal in-situ stress, and the minimum principal stress is not equal to the minimum in-situ stress. In this study, the mining-induced stress is taken as a research object and separated from the regional stress field. The remaining regional stress field can be approximated as in-situ stress field, i.e.:

$$\begin{cases} \sigma_1 \approx \sigma_H \\ \sigma_3 \approx \sigma_v \end{cases} \quad (7)$$

Therefore, σ_1 is selected in the range of 19.6–37 MPa (buried depth 800–1600 m) to study the roadway plastic zone. Additionally, the influence of various parameters on the shape and range of the roadway plastic zone is analysed.

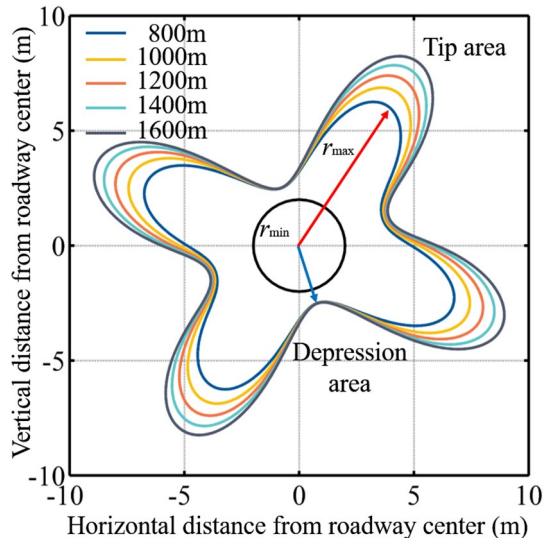
The in-situ stress environment of roadway under different buried depth is different. σ_1 and σ_3 increases with the buried depth. Five groups of different buried depths were selected to calculate in-situ stress to represent the regional principal stress. The results are shown in Table 2.

Other parameters are as follows: roadway radius $a = 2$ m, rock cohesion $c = 2$ MPa, internal friction angle $\varphi = 25^\circ$, mining-induced stress concentration coefficient $K = 5$, and in-situ stress deflection angle $\alpha = 18^\circ$. By introducing the parameters into Eq. (5), the variation of plastic zone depth with burial depth can be obtained, as shown in Fig. 4. Figure 4 shows the morphological evolution process of the plastic zone under the corresponding buried depth in Table 2.

As shown in Fig. 4, the plastic zone of the roadway, which can be divided into four tip areas and four depression areas, has different expansion characteristics in different directions. The entire plastic zone resembles a "petal shape". There are four tip areas in the directions of approximately 58° , 168° , 238° , and 328° (counter-clockwise being positive). Under these stress states, the plastic zone presents the characteristics of non-uniformity and symmetry. The non-uniformity is reflected in the great change in distance between the boundary of the plastic zone and the roadway wall at different angles. The symmetry is mainly reflected in the point symmetry of the plastic zone boundary about centre of the roadway (coordinate axis origin). As the buried depth increases from 800 to 1600 m, the plastic zone expands significantly at the four tips. By considering a tip at approximately 58° from the horizontal direction as an example, the radius of the plastic zone increases from 7.192 to 9.513 m with the buried depth increasing from 800 to 1600 m. The radius of plastic zone increased by 32.27%. In other areas except the tip part, the variation trend of the plastic zone boundary decreases with the increase in buried depth. In the depression area, the radius of plastic zone hardly increases with the buried depth. This is because the plastic zone at the tip is large. Accordingly, the surrounding rock in this region has low bearing capacity. When the increased stress caused by the buried depth acts on the surrounding rock, plastic yield obviously occurs. Then, a larger plastic zone is formed. However, the surrounding rock is relatively complete in the depression area. The rock mass in this area has good mechanical properties, and can resist the increase in stress caused by the increased buried depth. In other words, there is no obvious plastic zone expansion in this area. Additionally, some studies have shown that when there is a weak surface or yield region in the rock mass, the weak surface or yield

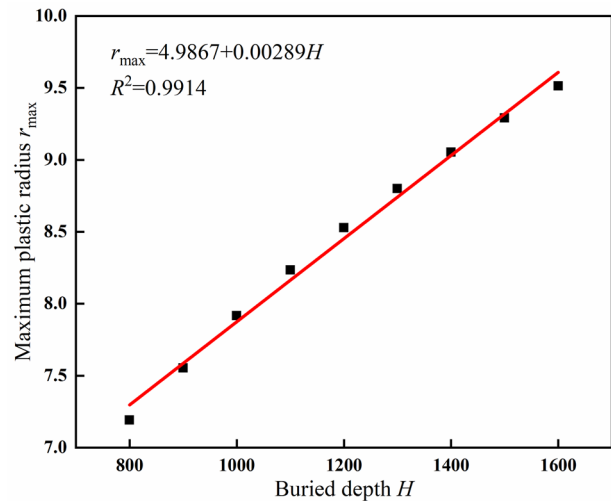
Table 2 In situ stress data under different buried depths

Buried depth/m	800	1000	1200	1400	1600
σ_1 /MPa	20.067	24.267	28.467	32.667	36.867
σ_3 /MPa	19.6	24.5	29.4	34.3	39.2

**Fig. 4** Variation law of plastic zone depth with buried depth (m)

region is more sensitive to stress change. The weak surface or yield region is more prone to damage and consumes energy, to protect the integrity of other rock mass areas. From the perspective of stress, the irregular shape of the plastic zone can be explained as follows: different θ angles correspond to different plastic zone radius. Taking in-situ stress and mining-induced stress as stress boundary, the stress state of any unit block near the roadway is different. Elements exceeding the strength of the rock mass will undergo plastic yielding. Therefore, the stress state of the unit block determines whether plastic yielding occurs. In the case of significant differences in stress between the two directions, there are also significant differences in the stress states of different unit blocks around the roadway. Therefore, an irregular plastic zone is formed.

The increase in buried depth will result in the obvious expansion of the plastic tip area. Based on the assumptions in Sect. 2, the relationship between the maximum radius r_{\max} of the plastic tip area and roadway buried depth H was fitted, as shown in Fig. 5. We found that with the increase in buried depth, the maximum radius of plastic zone increases approximately linearly. As far as this work was concerned, the fitting formula was found to be $r_{\max} = 4.9867 + 0.00289H$, whereas the correlation coefficient was $R^2 = 0.9914$. Figures 4 and 5 show that with the increase in buried depth, the plastic zone does not increase uniformly in equal proportion,

**Fig. 5** Relationship between maximum plastic radius and buried depth (m)

but increases locally along a certain direction. In addition, the maximum boundary of the plastic zone is predictable. When the geological conditions are known, the maximum radius of roadway plastic zone under different buried depths can be estimated using the fitting formula.

3.2 Evolution Law of the Plastic Zone Under Different Deflection Angles

The direction of in-situ stress is generally not completely horizontal or vertical. It is an angular deviation from the horizontal or vertical direction (Paul and Chatterjee 2011; Rajabi et al. 2010). The variation characteristics of the plastic zone of the surrounding rock when the deflection angle α changes from 0° to 90° are analysed in this section. The in-situ stress was selected based on the in-situ stress data with a buried depth of 1000 m, i.e., $\sigma_1 = 24.267$ MPa, $\sigma_3 = 24.5$ MPa, and the initial lateral pressure coefficient $\eta = 0.99$. The other parameters are: roadway radius $a = 2$ m, rock cohesion $c = 10$ MPa, internal friction angle $\varphi = 30^\circ$, and mining-induced stress concentration coefficient $K = 3$. The change process of the plastic zone in the process of in-situ stress direction deflection is shown in Figs. 6 and 7.

The evolution process of the plastic zone of the circular roadway during the change in in-situ stress deflection angle from 0° to 90° is shown in Figs. 6 and 7. As shown in Fig. 6, when the in-situ stress does not deflect, the plastic tip area of the roadway expands sharply to the deep area of the surrounding rock. The maximum plastic radius is approximately 12 m, which is 6 times that of the roadway radius. Meanwhile, the plastic zone was unsteady, which is likely to result in large deformation and failure of the roadway. This is because the mining-induced or disturbance stress ($K\sigma_v$)

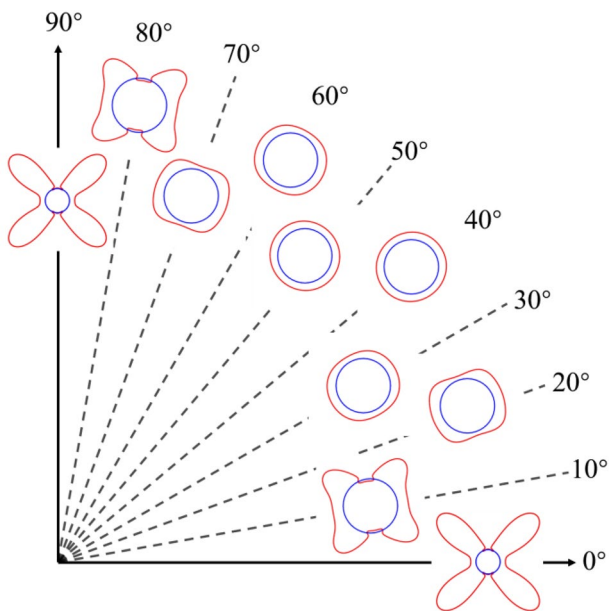


Fig. 6 Morphological evolution of the plastic zone under different in-situ stress deflection angles

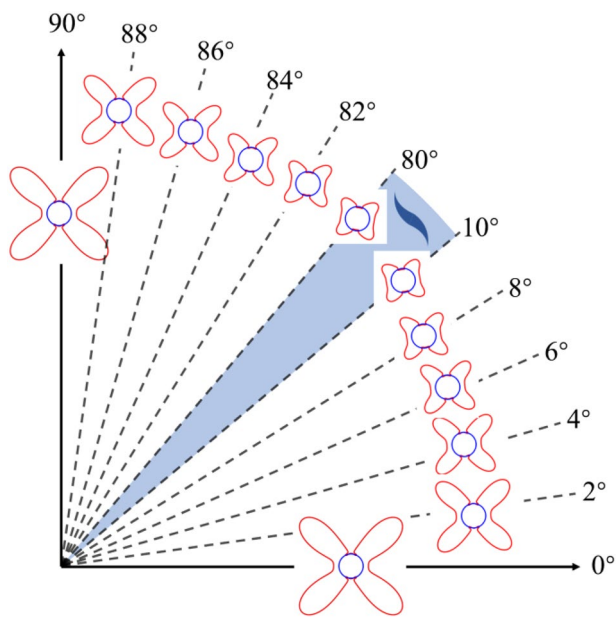


Fig. 7 Morphological evolution of the plastic zone from 0° to 10° and 80° to 90°

caused by mining or excavation acts vertically in the vertical direction, so the stress in the vertical direction after superposition is much greater than that in the horizontal direction. The surrounding rock enters plasticity in a large area under this extreme stress state. This shows that even when the difference between horizontal in-situ stress and vertical in-situ stress is very small, the existence of mining-induced

stress will produce irregular plastic zone in the roadway. It is embodied in the characteristics that the plastic zone varies greatly in the circumferential distribution range of the roadway and the local area fully extends to the depth of the rock mass, resulting in the roadway support is very difficult.

When the in-situ stress deflection is 10°, the plastic zone is still “petal shaped”, but the range of the plastic zone is significantly reduced. The maximum radius of the plastic zone is 4.2 m, which is 2.1 times the roadway radius. When the in-situ stress is deflected by 15°, the range of plastic zone is reduced further, and the overall shape is still “petal shaped”. The maximum boundary is approximately 3.35 m, which is approximately 1.67 times the roadway radius. When the in-situ stress deflection angle continues to increase from 15° to 25°, the plastic zone still is a “petal shaped”. However, its morphological characteristics degenerate gradually. The division of the 4 tip areas and the 4 depression areas fades gradually. When the in-situ stress deflection angle is 30°, the range of plastic zone continues to decrease. There are only four tip areas in the plastic zone shape, and there is no depression area. During this time, the shape of the plastic zone degenerates into an “ellipse shape”. With the increase in in-situ stress deflection angle, the shape of the plastic zone degenerates from an “ellipse shape” to a “circle shape”. When the in-situ stress deflection angle is 45°, the shape of the plastic zone can be regarded as a standard circle. This is because the mining-induced stress $K\sigma_v$ decomposes uniformly on the horizontal and vertical in-situ stress. The value is $\sqrt{2}/2K\sigma_v$, so η' , which does not increase significantly compared with η , is very close to 1. Therefore, the plastic zone of the roadway is “circular”. The range of the plastic zone is the smallest during this time. When the local stress deflection angle continues to increase, the shape of the roadway plastic zone evolves from a “circle shape” to an “ellipse shape”, and then develops into a “petal shape”. Correspondingly, the range of plastic zone increases gradually. Generally, when the in-situ stress deflection angle continues to increase from 45°, the variation characteristics of the shape and scope of the plastic zone are opposite to that of the decrease from 45°. β represents a random angle ($0^\circ < \beta < 45^\circ$), and the shape and range of plastic zone are roughly the same when the in-situ stress deflection angle is $45^\circ - \beta$ and $45^\circ + \beta$, but there are directional differences in the spatial position. Considering the in-situ stress deflection angles of 20° and 70° as an example ($\beta = 25^\circ$), the shape and range of the plastic zone under the two deflection angle states are basically the same. The corresponding maximum plastic boundaries were at is 3.16 m and 3.14 m. However, the plastic zone boundary is different in different spatial positions. By considering the horizontal right as the positive axis and counterclockwise as the positive direction, the maximum plastic boundary appears at approximately 60° in

the coordinate system when the in-situ stress deflection angle is 20° . The maximum plastic boundary appears at approximately 22° in the coordinate system when the in-situ stress deflection angle is 70° . Additionally, it can be observed from Fig. 6 that when the in-situ stress deflection angle changes from 0° to 10° , the plastic zone decreases significantly, and when it changes from 80° to 90° , the plastic zone expands substantially. It indicates that the plastic zone of roadway changes sharply in these two angle ranges. For this phenomenon, the variation of the plastic zone with the deflection angle in the range of 0° – 10° and 80° – 90° is drawn at an interval of 2° , as shown in Fig. 7. In the deflection angle ranges of 0° – 10° and 80° – 90° , a small angle change will result in a significant change in the range of plastic zone.

Finally, when the maximum and minimum in-situ stresses were assumed to be horizontal and vertical, the shape of the plastic zone obtained was quite different from that obtained by considering the actual direction of in-situ stress. In practical engineering, the magnitude and direction of in-situ stress need to be measured to guide the roadway surrounding rock support method and mining technology. The morphological evolution law of in-situ stress direction deflection on the roadway plastic zone is summarised as follows. As the in-situ stress deflection angle α increases from 0° to 90° , the morphological evolution process of the roadway plastic zone transforms from a “petal shape” ($0^\circ \leq \alpha \leq 20^\circ$)—“ellipse shape” ($20^\circ \leq \alpha \leq 40^\circ$)—“circle shape” ($40^\circ \leq \alpha \leq 50^\circ$)—“ellipse shape” ($50^\circ < \alpha \leq 70^\circ$)—“petal shape” ($70^\circ \leq \alpha \leq 90^\circ$). With respect to the evolution process of the roadway plastic zone range, when the in-situ stress deflection angle changes from 0° to 10° , the maximum boundary of plastic zone shows an obvious decrease, and then decreases slowly from 10° to 20° . Then, there is only a small fluctuation in the range of 20° – 70° and a sharp increase in the range of 70° – 90° , as shown in Fig. 8.

3.3 Evolution Law of the Plastic Zone Under Mining-Induced Stress

The variation characteristics of the plastic zone of the roadway surrounding rock were analysed when the stress concentration coefficient K changes from 3 to 5. The in-situ stress was selected based on the in-situ stress data with a buried depth of 1000 m, i.e., $\sigma_1 = 24.267$ MPa, and $\sigma_3 = 24.5$ MPa. The other parameters are as follows: roadway radius $a = 2$ m, rock cohesion $c = 10$ MPa, internal friction angle $\varphi = 25^\circ$, in-situ stress deflection angles α are 15° , 20° , and 25° . Figure 9 shows the response characteristics of the plastic zone with the change in mining-induced stress.

Figure 9 shows the development of the plastic zone of the roadway surrounding rock under different mining-induced

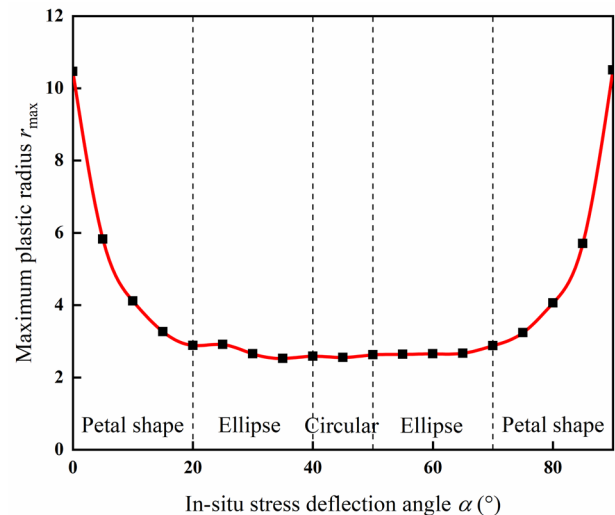


Fig. 8 Variation of maximum plastic zone radius with α

stress values. It shows that with the increase in mining-induced stress, the plastic zone of the roadway expands. With the increase in mining-induced stress (the increase in stress concentration coefficient K), the four tip areas in the roadway plastic zone expand to varying degrees under the three in-situ stress deflection angles. The increasing trend of the four sag areas is not obvious. Particularly, when the in-situ stress deflection angle $\alpha = 15^\circ$, the stress concentration coefficient changes from 3 to 5 and the four tip areas of the plastic zone increase approximately linearly. The maximum radius of the plastic zone increased from 4.02 to 6.71 m. When the in-situ stress deflection angle is 20° , with the increase in stress concentration coefficient, the four tip areas of the roadway plastic area increased to a certain extent. It was far less intense than that when the in-situ stress deflection angle was 15° . At the same time, the “petal shape” feature of the roadway plastic zone is obvious: when the stress concentration coefficient $K = 3$, the shape of the plastic zone is closer to the chamfered rectangle, and the maximum boundary of the plastic area is 3.34 m. With the increase in K , the boundary between the tip area and depression area is gradually clear, and the “petal shape” gradually appears. The maximum boundary of the plastic zone is 4.33 m. When the in-situ stress deflection angle is 25° , the influence amplitude of mining-induced stress is further reduced. The shape and range of plastic zone do not change obviously under different stress concentration coefficients. Finally, the following conclusions can be drawn. The influence of mining-induced stress on the roadway plastic zone is more intense when the angle between mining-induced stress and in-situ stress is small.

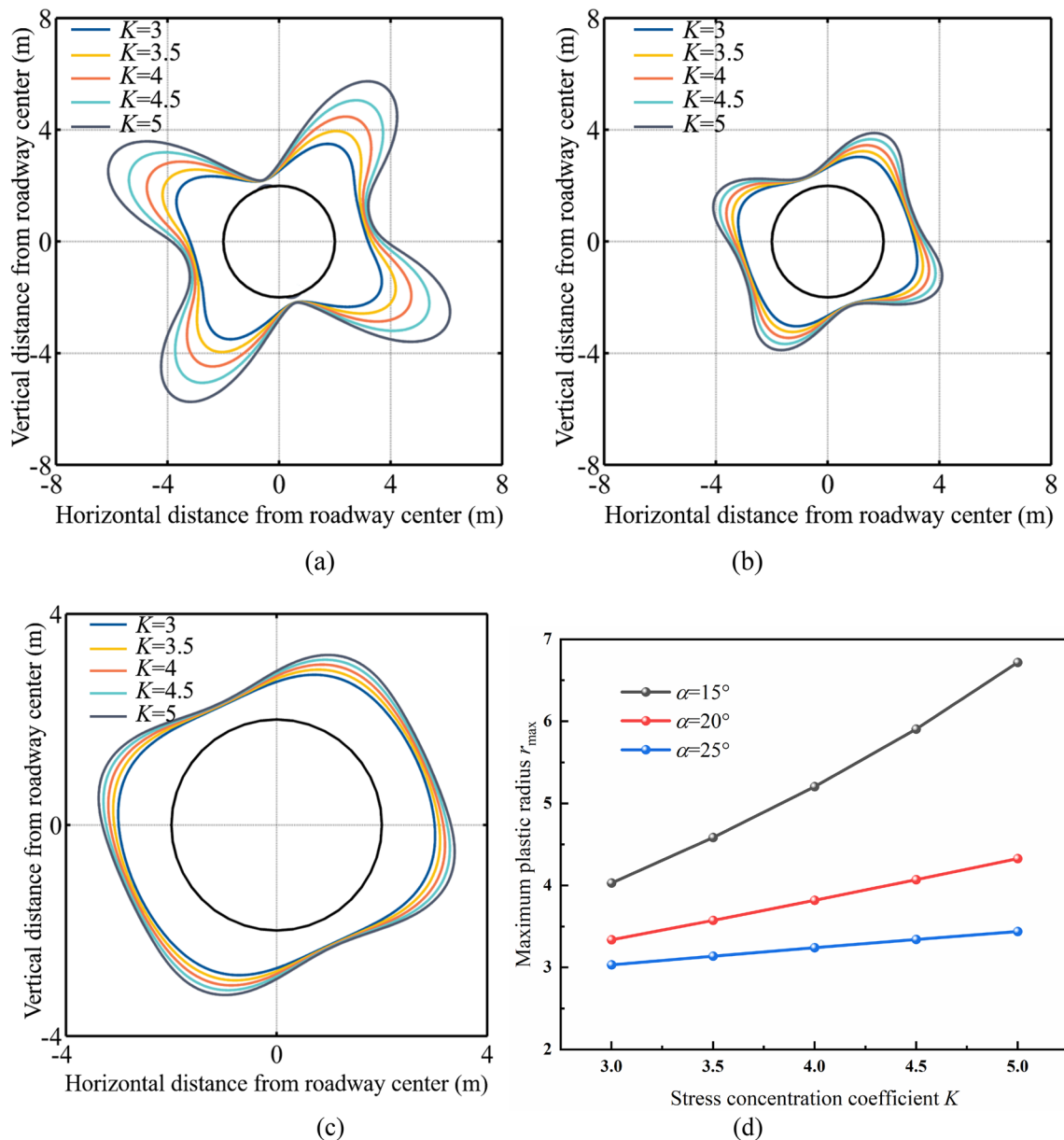


Fig. 9 Shape of the plastic zone under different stress concentration coefficients: **a** $\alpha = 15^\circ$, **b** $\alpha = 20^\circ$, **c** $\alpha = 25^\circ$, and **d** relationship between r_{max} and K

3.4 Evolution Mechanism

The influence of in-situ stress deflection angle α and mining-induced stress σ' on the shape and range of the roadway plastic zone is analysed in the previous section. In this section, we will explain the action mechanism from the perspective of mechanical analysis. The internal cause of plastic zone is the response process of rock mass when various stresses such as in-situ stress and mining-induced stress, are applied to the rock mass. According to the above analysis, in-situ stresses σ_1 and σ_3 , mining-induced stress σ' , in-situ stress deflection angle α and the self attributes of rock mass (such

as cohesion c , internal friction angle φ , etc.) are all factors affecting the shape and range of the plastic zone (Zuo et al. 2009). Among them, in-situ stresses σ_1 and σ_3 , mining-induced stress σ' and in-situ stress deflection angle α are the external factors. These are the decisive factors for the formation of the plastic zone. The attribute of rock mass is an internal cause. Under the condition of the same external stress, the internal cause controls the shape and range of the plastic zone. Therefore, considering the external decisive factors, the shape and range evolution mechanism of the roadway plastic zone from the perspective of mechanical action mechanism is analysed in this section.

The existing research results show that when the roadway is under the condition of two-way equal pressure ($\eta = 1$), the shape of the plastic zone is circular. However, under the condition of two-way unequal pressure, the plastic zone presents an irregular shape. The specific shape depends on the lateral pressure coefficient η . Based on the research results, the mechanical principle of the evolution process of the roadway plastic zone is further discussed. Thus, the equivalent lateral pressure coefficient is defined as the ratio of horizontal stress to vertical stress after the complex superposition of in-situ stress and mining-induced stress. The expression is shown in Eq. (3).

The expression of mining-induced stress is:

$$\sigma' = K\sigma_v = K\sigma_3 \quad (8)$$

Therefore, the expression of η' can be further expressed as:

$$\eta' = \frac{\sigma_1 + K\sigma_3 \sin \alpha}{\sigma_3 + K\sigma_3 \cos \alpha} = \frac{\eta + K \sin \alpha}{1 + K \cos \alpha} \quad (9)$$

Equation (9) shows that the initial lateral pressure coefficient η , in-situ stress deflection angle α and stress concentration coefficient K jointly affect the equivalent lateral pressure coefficient η' . In other words, these parameters jointly determine the shape of the plastic zone. Figure 10 depicts the evolution law of equivalent lateral pressure coefficient η' during the gradual change in initial lateral pressure coefficient η and in-situ stress deflection angle α when $K=3, 4$, and 5. The two abscissas represent the initial lateral pressure coefficient η and in-situ stress deflection angle α . η ranges from 0.5 to 3, and α ranges from 0° to 90° .

It can be observed from Fig. 10 that the equivalent lateral pressure coefficient η' increases with the increase in stress concentration coefficient K . When the initial lateral pressure coefficient η and in-situ stress deflection angle α are small, the increasing trend of the equivalent lateral pressure coefficient η' is relatively slow when the stress concentration coefficient K changes from 3 to 5. This means that the shape of the corresponding plastic zone hardly changes. As the initial lateral pressure coefficient η and in-situ stress deflection angle α increases, the increase in K significantly increases the equivalent lateral pressure coefficient η' . For example, when $\eta=3$ and $\alpha = 90^\circ$, η' increases from 6 to 8 as K increases from 3 to 5. This means that the shape of the corresponding plastic zone changed significantly. When the in-situ stress deflection angle α is in the range of 0° – 45° , the change in surface is relatively gentle. When α changes in the range of 45° – 90° , the change range of the surface increases significantly, i.e., η' increases significantly. η' determines the shape of the plastic zone, i.e., when the angle of α is large, a small increment will lead to obvious changes in the shape of the plastic zone. In conclusion, α , η and K jointly determine

the size of η' , and the action law is relatively consistent. In other words, η' increases with the increase in α , η , and K , but the influence degree is different. η' , which is very sensitive to α , increases exponentially as α increases. Particularly, when $\alpha > 45^\circ$, a small increment will significantly increase η' . η' increases approximately linearly with the increase in η and K , and the increase range is far less severe than that of α . In particular, when α is between 0° – 10° and 80° – 90° , the plastic zone changes sharply. It means that the plastic zone has undergone dramatic evolution in shape and scope. Take the parameters in Sect. 3.2 as an example, in the $0^\circ < \alpha < 10^\circ$ range, $0.2475 < \eta' < 0.3821$; in the $80^\circ < \alpha < 90^\circ$ range, $2.5934 < \eta' < 3.99$. In these two intervals, the difference between σ'_1 and σ'_3 is large, which results in the obvious changes in the shape and range characteristics of the plastic zone during the change process. The results are in good agreement with the plastic zone changes shown in Fig. 7.

As mentioned above, the existing research results suggest that η controls the shape of the plastic zone. However, the equivalent lateral pressure coefficient η' controls the shape of the plastic zone under the mining-induced stress and in-situ stress direction deflection. Therefore, not only η , but K and α also control the shape of the plastic zone. It means that given a maximum principal stress σ_1 and minimum principal stress σ_3 , the change in in-situ stress direction and mining-induced stress will cause a change in the plastic zone shape. To explore the specific influence of η' on the plastic zone, the relevant parameters are: $\sigma_1=25$ MPa, $\sigma_3=20$ MPa, $\eta=1.25$, $c=5$ MPa, $\varphi=30^\circ$, and $K=3, 4$ and 5. When α changes, η' changes along with α . Then, the value of η' can be obtained. The plastic zone boundary can be calculated according to Eq. (5) subsequently. Taking the ratio of the maximum radius r_{\max} to the minimum radius r_{\min} of the plastic zone as the longitudinal axis and η' as the transverse axis, the relationship between r_{\max}/r_{\min} and η' is obtained, as shown in Fig. 11. η' can be calculated using Eq. (9).

Figure 11 shows the variation law of r_{\max}/r_{\min} with η' . As observed from the Fig. 11, r_{\max}/r_{\min} first decreases and then increases as η' increases, and the minimum value is taken when $\eta' = 1$. In the theoretical calculation process, we found that when η' is greater than the minimum critical line and less than 0.55, r_{\max}/r_{\min} rapidly decreases to approximately 1.3. The shape of the plastic zone is “petal shaped”. In the range of $0.55 < \eta' < 0.9$, r_{\max}/r_{\min} slowly decreases from 1.3 to approximately 1.1, and the plastic zone of the roadway degenerates into an “ellipse shape”. In the range of $0.9 < \eta' < 1.1$, r_{\max}/r_{\min} has a process of slow decline and rise. The minimum of r_{\max}/r_{\min} value is 1.0, which is also the lowest point of the entire curve. The plastic zone further degenerates into a “circle shaped”. In the range of $1.1 < \eta' < 1.7$, r_{\max}/r_{\min} increases from 1.1 to approximately 1.25. The plastic zone re evolves into an “ellipse shape”. In the range of $1.7 < \eta' < 2.5$, r_{\max}/r_{\min} increased from 1.25

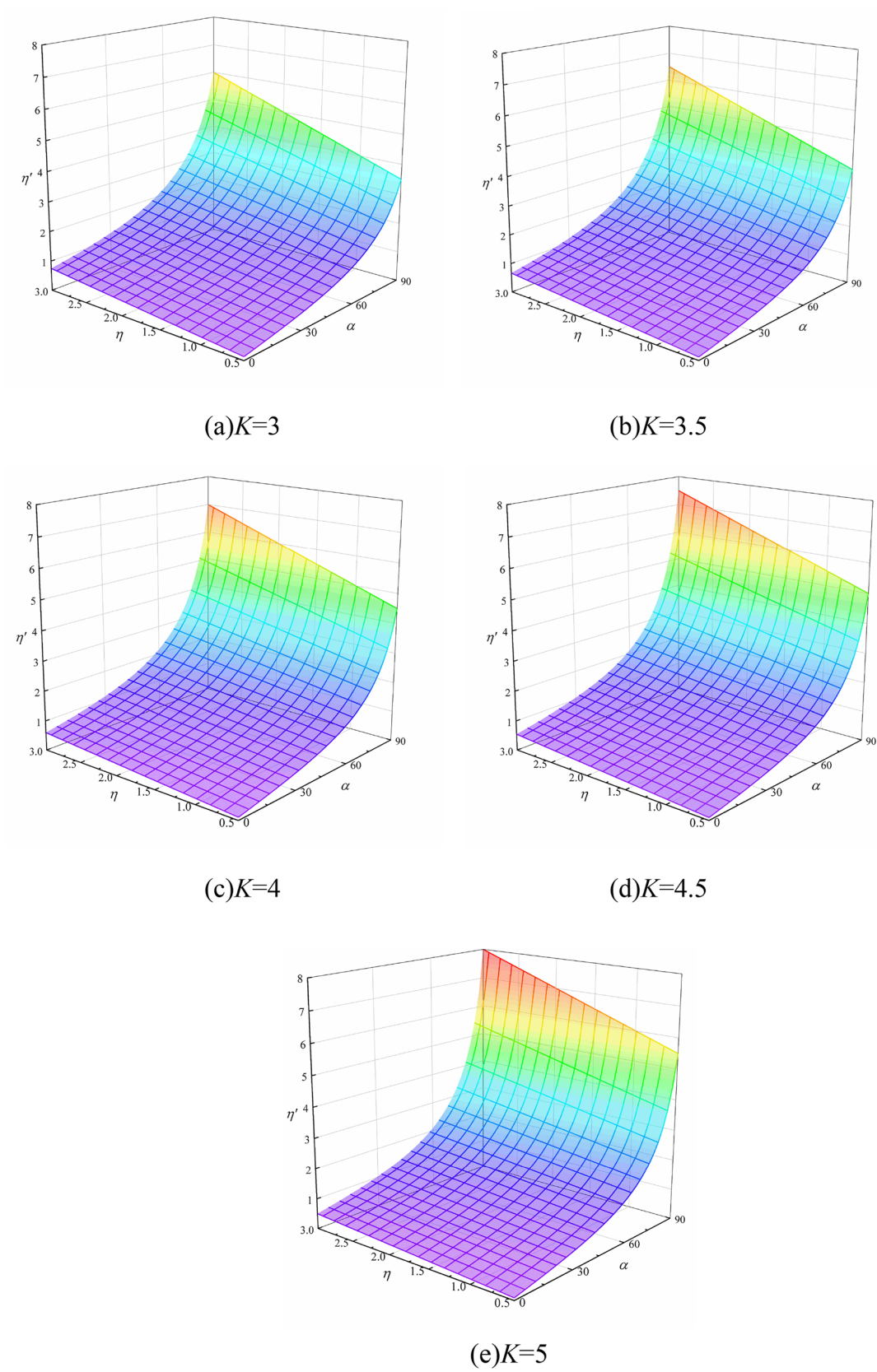


Fig. 10 Relationship between equivalent lateral pressure coefficient η' and initial lateral pressure coefficient, and the in-situ stress deflection angle and mining-induced stress

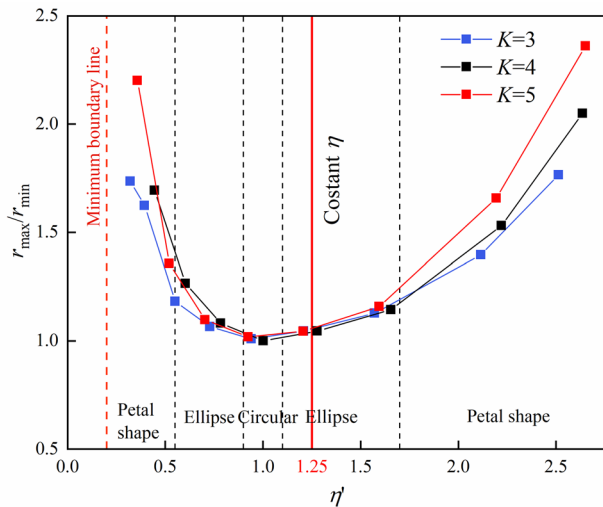


Fig. 11 Effect of equivalent lateral pressure coefficient η' on the shape of the plastic zone

to approximately 2. The plastic zone evolved into a “petal shape”. When η' continues to increase, the stress around the roadway is highly concentrated. During this time, the large-scale rock mass enters plasticity and has no plastic zone boundary. If the cohesion c and internal friction angle φ of rock mass increase appropriately, the plastic zone is still “petal shaped”, which will not be discussed in this study. When K increases gradually, r_{\max}/r_{\min} also increases, and the curve is more steep. This indicates that the increase in K makes the morphological characteristics of the plastic zone more obvious. It can be observed that when η remains unchanged, the changes in α and K will completely change the plastic zone morphology.

4 Numerical Simulation of Non-orthogonal Failure

To verify the correctness of the theoretical analysis results, the numerical simulation software FLAC^{3D} was used to simulate the non-orthogonal theoretical model. The influence of different stress deflection angles and different stress concentration coefficients on the roadway plastic zone was mainly analysed. The model is shown in Fig. 12. The length and width of the model are 40 m, thickness is 10 m, and roadway radius is 2 m. The roadway is generated by the cylinder command. The surrounding rock mass is generated by radcylinder command. On the model boundary, each grid represents 1 m. The Mohr–Coulomb failure criterion was adopted in the model. When the unbalanced force ratio reaches 1×10^{-5} , the iteration calculation is terminated. According to Eqs. (1) and (2), the values of σ'_1 and σ'_3 were input into the model to obtain the plastic zone shape when

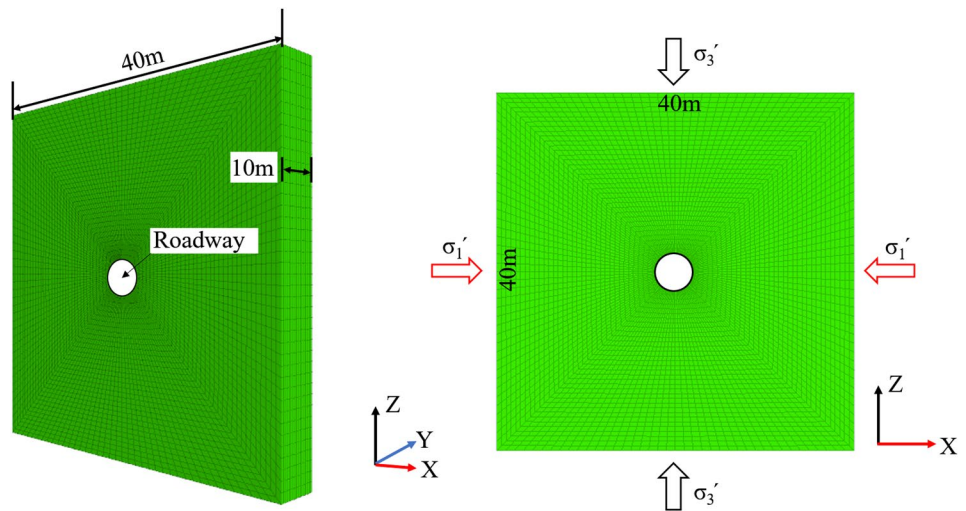
the in-situ stress deflection angle was α . The spatial position distribution of the corresponding plastic zone can be obtained when the model is rotated counter-clockwise by α at the end of the calculation.

4.1 Different Buried Depths

The following parameters are used in this section: roadway radius $a = 2$ m, rock cohesion $c = 20$ MPa, internal friction angle $\varphi = 30^\circ$, stress concentration coefficient $K = 5$, in-situ stress deflection angle $\alpha = 20^\circ$. The roadway plastic zone under different buried depths was simulated. The variation of the plastic zone with the buried depth is shown in Fig. 13. It can be seen that the range of the roadway plastic zone increases with the increase in buried depth. When the buried depth is 800 m, the range of the roadway plastic zone is small. The plastic zone is “ellipse shaped”. When the buried depth increases gradually, the plastic zone increases significantly. When the buried depth increases to 1600 m, the roadway plasticity evolves into “petal shape”, and the range of the plastic zone increases significantly. Compared with the theoretical calculation results, the range and morphological evolution of the plastic zone are in good agreement. The range of the plastic zone in the numerical simulation is generally slightly larger than that in the theoretical calculation, which is mainly caused by grid division. Even if the grid division is more precise, it cannot replace the lines obtained in the theoretical calculation. The area of the plastic zone in theoretical calculation and numerical simulation was extracted. The variation law with the increase in burial depth is shown in Fig. 14. When the burial depth is within the range of 800–1400 m, the relative error between the two is basically within 15%. Only when the burial depth increases to 1600 m, the results calculated by the two methods will be significantly different.

The same parameter setting as Sect. 3.2 is selected to simulate the evolution trend of roadway plastic zone. The evolution trend of roadway plastic zone during the change in in-situ stress deflection angle from 0° to 90° was shown in Figs. 15 and 16. The shape and range of the plastic zone under different in-situ stress directions were studied. By comparing Figs. 6 and 7, we found that the plastic zone under the same in-situ stress deflection angle α via theoretical analysis and numerical simulation has good consistency in shape and range. Under different in-situ stress deflection angles, the variation trend of the plastic zone is also the same as that of the theoretical analysis. It can be observed from the figure that the plastic zone mainly suffers shear failure, and local tensile failure occurs in a small range at the edge of the roadway when the in-situ stress deflection angles are 0° , 10° , 80° and 90° . When the in-situ stress deflection angle is 0° – 40° , the state of the plastic

Fig. 12 Geometric dimensions and boundary conditions of the numerical model



zone is mainly “shear-n shear-p”. This means that the rock mass in the plastic zone is still shearing at the end of the simulation calculation. When the in-situ stress deflection angle ranges from 40° to 90°, the state of the plastic zone is mainly “shear-p”. This suggests that the rock mass in the plastic zone has ended the shear process at the end of the simulation calculation. This phenomenon shows that when the in-situ stress deflection angle is large, the surrounding rock has advanced more into plasticity. This is because in the process of increasing the in-situ stress deflection angle, σ_1' continues to increase and σ_3' continues to decrease. Thus, the corresponding Mohr circle intersects with the strength

envelope first. Therefore, it enters plasticity first. In terms of shape and scope, the simulation results are consistent with the theoretical analysis results, which verifies the correctness of the theoretical analysis of the roadway plastic zone. In the small angle variation range, the numerical simulation is in good agreement with the theoretical results, as shown in Figs. 7 and 16. The results verify the rationality of the mechanism analysis again in Sect. 3.4.

4.2 Different Lateral Pressure Coefficients

As discussed, when the in-situ stress and mining-induced stress are orthogonal, the lateral pressure coefficient η controls the shape of the plastic zone. However, when the in-situ stress and mining-induced stress are non-orthogonal, the equivalent lateral pressure coefficient η' controls the shape of the plastic zone. To study the main control effect

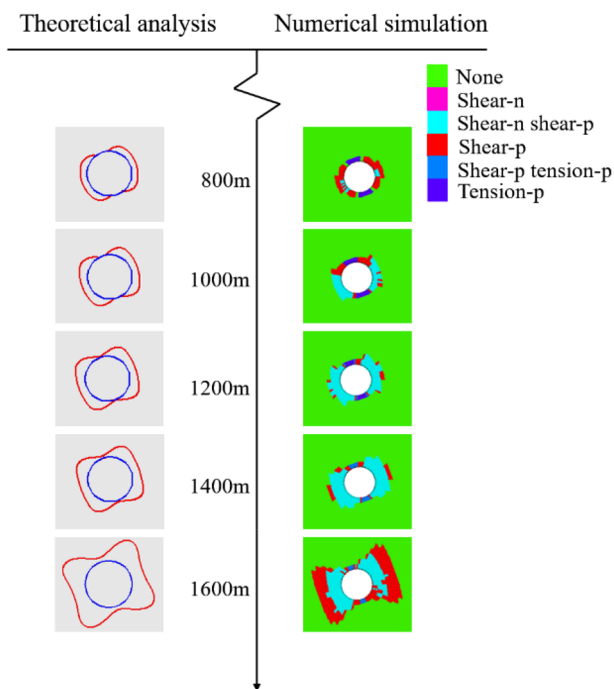


Fig. 13 Comparison between numerical simulation and theoretical calculation of the plastic zone shape under different buried depths

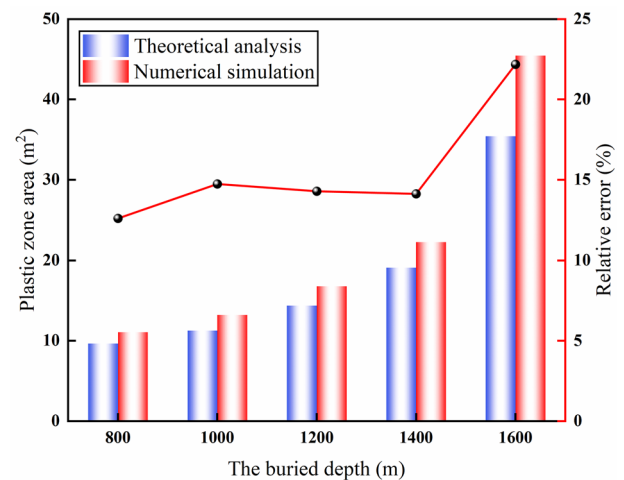


Fig. 14 Comparison of the numerical simulation and theoretical calculation of the plastic zone area under different buried depths

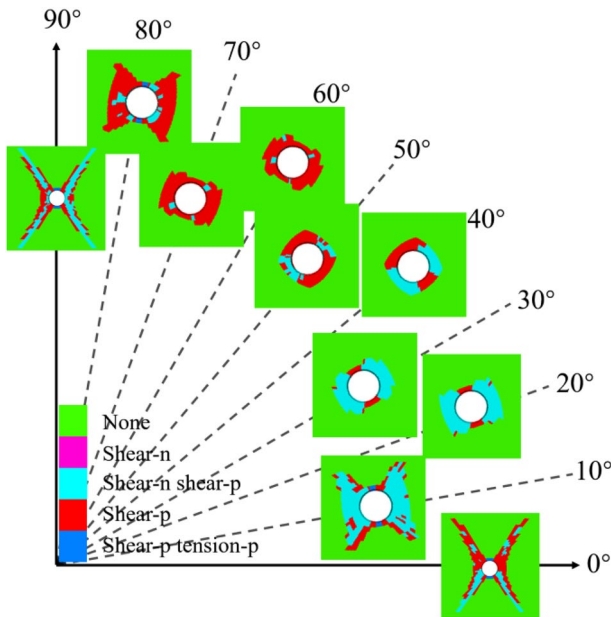


Fig. 15 Numerical simulation results of the plastic zone morphological evolution at different in-situ stress deflection angles

of equivalent lateral pressure coefficient η' , the development law of the plastic zone under orthogonal and non-orthogonal states of in-situ stress and mining-induced stress under different initial lateral pressure coefficients is simulated, respectively, as shown in Fig. 17. The other parameters are: rock cohesion $c = 20$ MPa, the friction $\varphi = 30^\circ$, stress concentration coefficient $K = 3$, regional vertical principal stress $\sigma_3 = 24.5$ MPa, and initial lateral

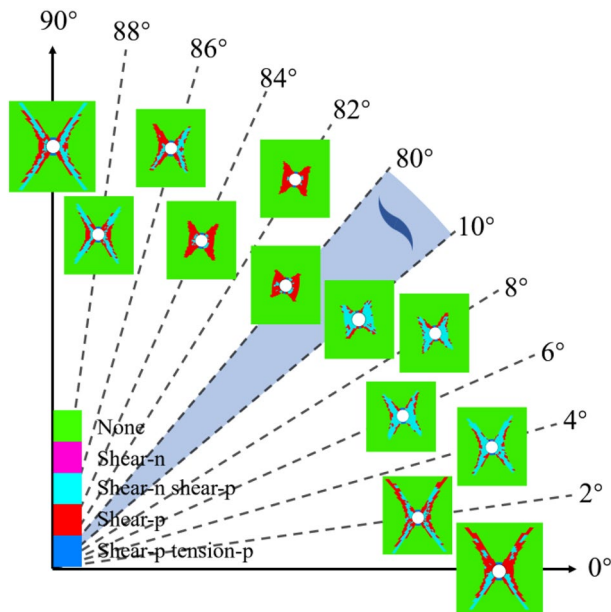


Fig. 16 Numerical simulation results of the plastic zone morphological evolution from 0° to 10° and 80° to 90°

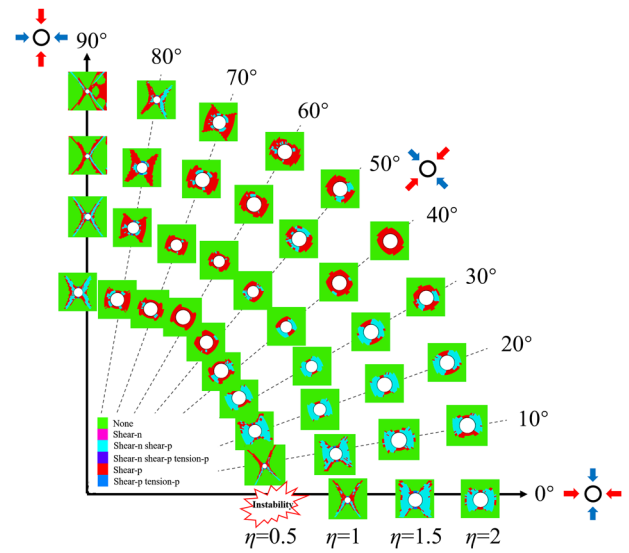


Fig. 17 Distribution law of plastic zone under different lateral pressure coefficients

pressure coefficients $\eta = 0.5, 1, 1.5,$ and 2 . As shown in Fig. 17, even if the initial lateral pressure coefficient remains unchanged with the change in in-situ stress deflection angle α , the shape of the plastic zone undergoes a cyclic change of “petal shape”—“ellipse shape”—“circle shape”—“ellipse shape”—“petal shape”. This further shows that it is difficult to accurately judge the plastic zone shape only by the initial lateral pressure coefficient without considering the actual stress state of the roadway. The equivalent lateral pressure coefficient considering the stress state of the roadway can accurately reflect the plastic zone shape of the roadway. When the in-situ stress and mining-induced stress are orthogonal (in-situ stress deflection angle $\alpha = 0^\circ$), the range of the roadway plastic zone converges gradually and the morphology gradually degenerates as the lateral pressure coefficient increase. When $\eta = 0.5$, the corresponding stress σ'_1 and σ'_3 have a large difference. The roadway has been completely unstable. The roadway has been completely destroyed. The simulation calculation has been unable to reach the equilibrium state. When $\eta = 1$, the plastic zone has a “thin petal shape”. When $\eta = 1.5$, the shape of the plastic zone evolves into a “petal shape”. When $\eta = 2$, the shape of the plastic zone degenerates into an “ellipse shape”. In the non-orthogonal state, the plastic zone does not change so violently. For example, when the in-situ stress deflection angle is $\alpha = 70^\circ$, η changes from 0.5 to 2 , the plastic zone changes from an “ellipse shape” to a “petal shape”. Therefore, it is not accurate to use the initial lateral pressure coefficient to determine the plastic zone. Figure 17 reflects the variation law of the roadway plastic zone in different in-situ stress

environment in coal mining. The approximate range of the roadway plastic zone corresponding to any geological condition and mining condition can be found. Thus, the research results have certain universality.

5 Discussion and Case Study

5.1 Plastic Zone Characteristics

The instability and failure of roadway are the result of the coupling of multiple factors. External factors such as in-situ stress, fault, structure, etc. Faults and structures act on the roadway in a way that causes changes in the stress field. Internal factors such as layers, roof and floor lithology, water content, etc. It is difficult to determine failure modes will occur in the roadway under such complex factors. The research has been simplified to some extent. Starting from the fundamental factors of stress environment changes. Other factors that may affect the instability and failure of the roadway were not considered.

The effects of different initial lateral pressure coefficient, equivalent lateral pressure coefficient, in-situ stress deflection angle, and mining-induced stress concentration coefficient on the range and shape of the roadway plastic zone were analysed and studied. On this basis, the theoretical and numerical results were further compared. According to different influencing factors, Fig. 18 depicts the different spatial positions and shape characteristics of the roadway plastic zone.

When the regional principal stress σ_1 is large, the ratio of two-dimensional stress decreases after the stress redistribution in the process of the roadway excavation, and the plastic zone of roadway will converge. As shown in Fig. 18a, when σ_3 remains unchanged and the initial lateral pressure coefficient increases from 1 to 3, the stress state of the area tends to be uniform under mining-induced stress. In other words, the equivalent lateral pressure coefficient gradually tends to be 1, and the shape of the plastic zone gradually degenerates from a “petal shape” to an “ellipse shape”, and then to a “circle shape”. Additionally, the range of the plastic zone reduces gradually. In the stratum with large lateral pressure coefficient, the support after roadway excavation with non-orthogonal in-situ stress and mining-induced stress is easier. When the initial lateral pressure coefficient remains unchanged and the equivalent lateral pressure coefficient changes from 0.5 to 2, as shown in Fig. 18b, the change trend of the roadway plastic zone is “petal shaped”, “circle shape”, “ellipse shape” and “petal shaped”. The “petal shape” has obvious directionality, and the tip area is generally located at the angular bisector of the angle of the equivalent principal stress.

The non-normality of in-situ stress and mining-induced stress will significantly affect the shape and range of the plastic zone. Different non-orthogonal angles will result in different mechanical states of the roadway, as shown in Fig. 18c. When the deflection angle is 10° , 45° , and 80° , the magnitude and direction of the principal stress in the roadway area are different, and the plastic zones are “petal shaped”, “circle shape”, and large “petal shaped” respectively. The range of the plastic zone is the smallest when the in-situ stress deflection is 45° , and largest when the in-situ stress deflection is 80° . Moreover, the mining stress in the non-orthogonal state will significantly affect the plastic zone. As shown in Fig. 18d, when the mining-induced stress concentration coefficient increases from 3 to 5, the shape of the roadway plastic zone is “petal shape”, but the range increases significantly.

The evolution law of the roadway plastic zone under complex stress state was analysed in this study. Under different stress states, the plastic zone of the roadway experiences the cyclic evolution from the “petal shape”—“ellipse shape”—“circle shape”—“ellipse shape”—“petal shape”. The plastic zone of the roadway shows different forms under different geological conditions and working conditions. When the in-situ stress state and mining technology of the stratum where the roadway is located are determined, the initial lateral pressure coefficient, in-situ stress deflection angle and mining stress are determined. The approximate range of the roadway plastic zone can be obtained by substituting the parameters into the proposed calculation method. In many literatures, the mechanical factor considered by researchers is only the regional primary in-situ stress field. In this study, the morphology of the plastic zone is the result of the coupling of the regional in-situ stress field and mining-induced stress field. The mechanical mechanism is more in line with the stress state in engineering practice. Second, without changing the magnitude of various forces, non-orthogonal angle changes can also produce a “petal-shaped” plastic zone and the morphological evolution of the plastic zone, which has not been investigated in the literature. Finally, the “petal-shaped” plastic zone is only one manifestation of the results. The entire process of cyclic evolution of the plastic zone is the focus of this study, so the results of this study are more applicable to engineering.

5.2 Case of Verification in the Hudi Coalmine

Research results on the plastic zone of the roadway envelope are mainly focused on theoretical calculations and numerical simulations, and there are few research results that can verify the scope of the plastic zone in conjunction with engineering practice. It is difficult to investigate the plastic zone of the roadway directly. Generally speaking, the range of plastic

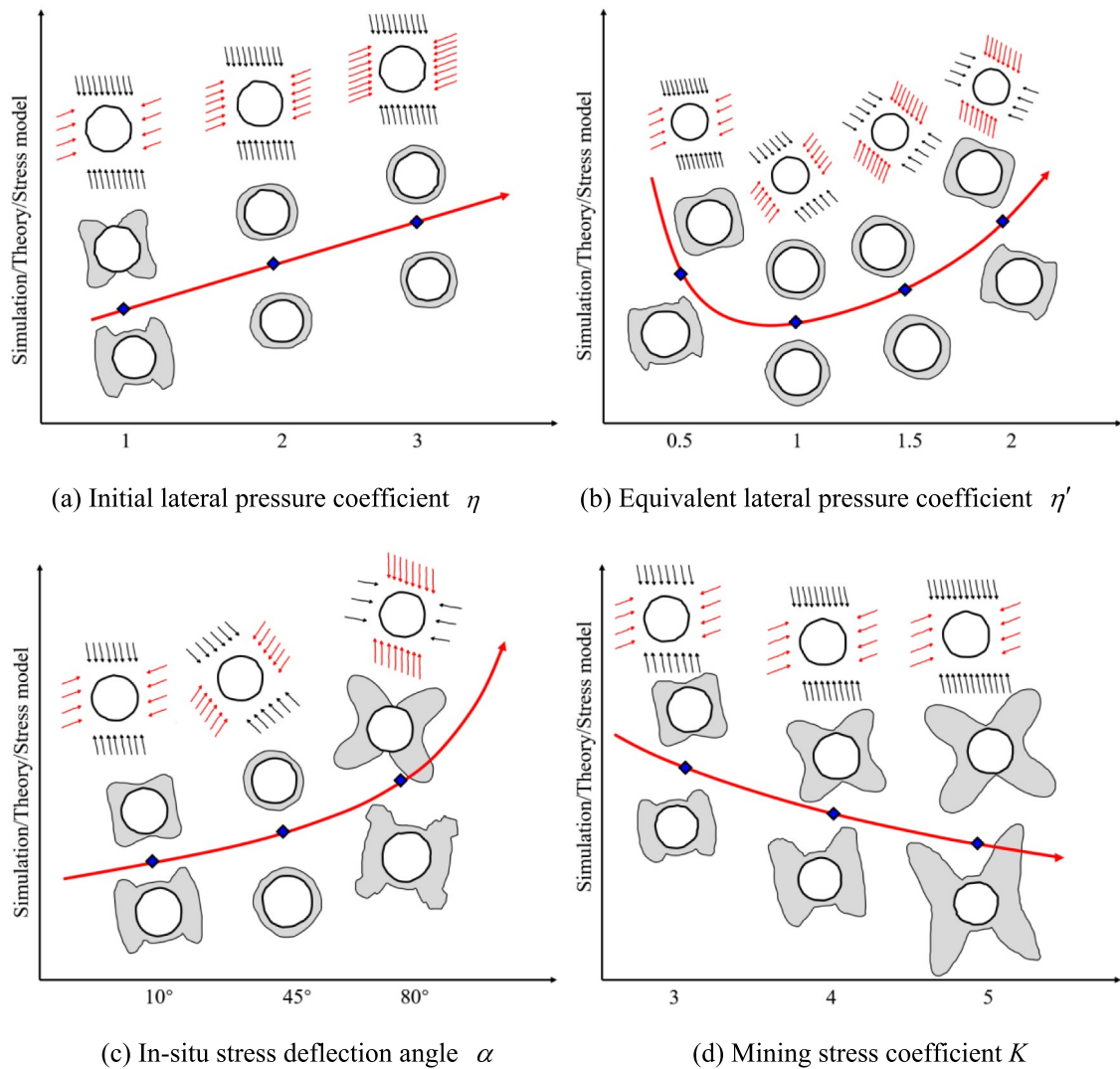


Fig. 18 Schematic diagram of the relationship between theoretical calculation, numerical simulation, and stress model

zone is related to the deformation and failure of roadway surface. The larger the plastic zone is, the more serious the damage and deformation of the corresponding roadway surface will be. In the area with small plastic zone, the damage and deformation of the corresponding roadway surface are slight. Nevertheless, the plastic zone has a certain correspondence with the loose circle. Where the plastic zone is large, the loose circle is correspondingly larger; where the plastic zone is small, the loose circle is smaller. Therefore, the indirect verification of the plastic zone can be performed from the loose circle. The results were verified by selecting the engineering background of 1305 bottom drainage roadway in the Hudi mine, Shanxi province, China.

By combining laboratory tests, stress monitoring and mine pressure manifestation data, the mechanical parameters

and stress concentrations of the 1305 bottom drainage roadway were obtained, as shown in Table 3.

The in-situ stress test was performed in the Hudi mine using the stress release method, and the in-situ stress test results of 1305 bottom drainage roadway are shown in Table 4.

Combined with the in-situ stress test results of the Hudi mine, the distribution of the overall in-situ stress direction of the mining area and the specific in-situ stress state of the 1305 bottom drainage roadway were obtained, as shown in Fig. 19.

According to the rock parameters, mining-induced stress and in-situ stress data, the plastic zone distribution of 1305 bottom drainage roadway calculated by the proposed method is shown in Fig. 20. It can be observed that deformation or

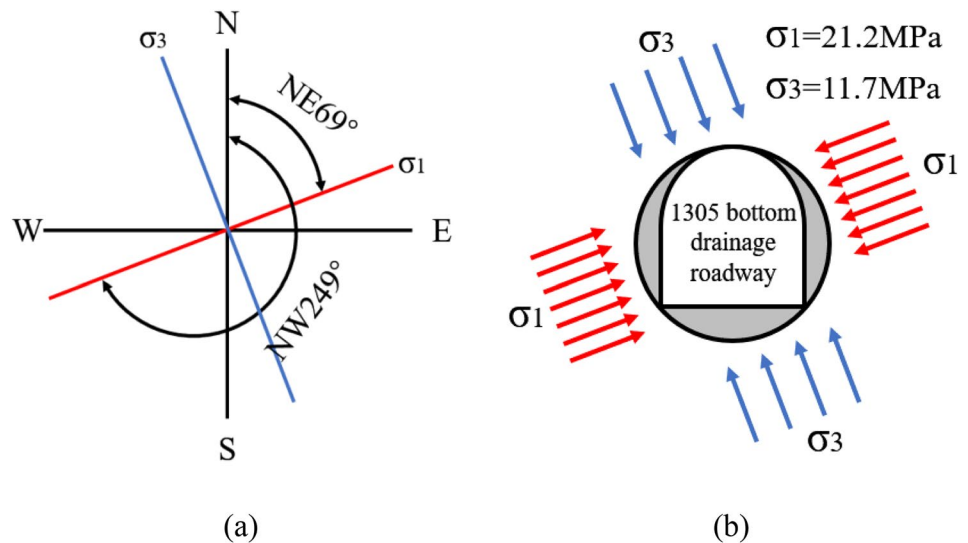
Table 3 Mechanical parameters and stress concentration coefficient of roadway

Roadway	Lithology	Cohesion c (MPa)	Internal friction angle φ ($^{\circ}$)	Elastic modulus E (GPa)	Poisson's ratio μ	Concentration coefficient K
1305 bottom drainage roadway	Mudstone	2.58	30	4.36	0.22	2.1

Table 4 In situ stress measurement results of 1305 bottom drainage roadway

Location	Principal stress classification	Principal stress value (MPa)	Azimuth ($^{\circ}$)	Dip angle ($^{\circ}$)
1305 bottom drainage roadway	Maximum principal stress σ_1	21.2	248.1	24.1
	Intermediate principal stress σ_2	15.2	43.8	63.7
	Minimum principal stress σ_3	11.7	153.8	9.6

Fig. 19 In-situ stress of Hudi mine: **a** in-situ stress direction of the mining area; **b** in-situ stress state of 1305 bottom drainage roadway



damage areas are most likely to occur in (a), (b), (c), and (d) areas of the roadway, and they show obvious asymmetry. The failure pictures of the field survey of the roadway are shown in Fig. 21. In (a), (b), (c), and (d) areas, the roadway shows obvious unsymmetrical deformation damage. The plastic zone calculated theoretically is in good agreement with the roadway deformation measured in the field, indicating that the plastic zone calculation method proposed in this study is consistent with the engineering reality and can be applied in the field.

Additionally, the distribution range of the loose circle of the roadway was tested by the acoustic method. Two sections were selected at 295 m and 310 m of the bottom drainage roadway for testing. Two holes were drilled in each roadway section, with hole diameter is 42 mm and hole depth is 4 m. The holes were symmetrically arranged along the central

axis of the roadway. The layout of the roadway and loose circle test points are shown in Fig. 22. The section drilling arrangement scheme is shown in Fig. 23.

The measured depth of the loose circle for each hole was counted and the results were compared with the theoretical calculation, as shown in Table 5.

As observed from Table 5, the loose circle field test results of the 1305 bottom drainage roadway were between 1.0 and 1.3 m, and the plastic zone results of the theoretical calculation were between 1.62 and 1.86 m. The ratio interval between them is between 0.6 and 0.7, which is consistent with the distribution law of loose circle and plastic zone range. The comparison data show that the calculation method of the plastic zone under stress deflection in this study is reasonable and correct.

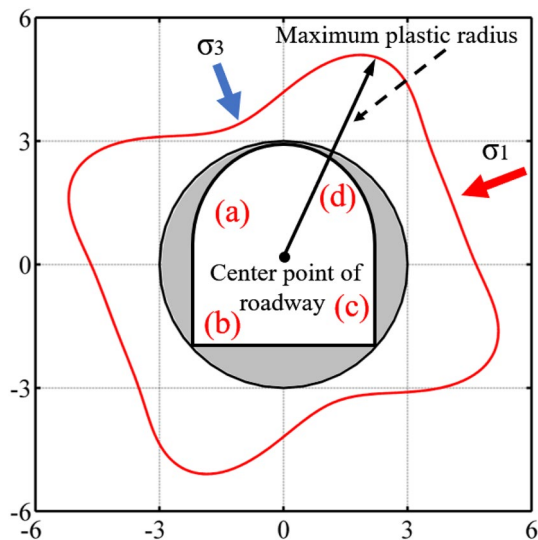


Fig. 20 Distribution of plastic zone and dangerous failure zone of the 1305 bottom drainage roadway

6 Conclusions

Figure 24 is the Research flowchart, which clearly and directly illustrates the process of this research. In this study, the variation law of the plastic zone of roadway surrounding rock under the condition of non-orthogonal in-situ stress and mining-induced stress was studied. Combined with the results of theoretical analysis, numerical simulation, and field verification, we arrived at the following conclusions:

- (1) The stress model of the roadway surrounding rock under the non-orthogonal state of in-situ stress and mining-induced stress was established. The boundary equation of the plastic zone was solved. The distribution law of the roadway plastic zone was studied under different buried depth, different in-situ stress direction, and different mining-induced stress. In terms of morphology, the plastic zone presents the evolution phenomenon from “petal shape”—“ellipse shape”—“circle shape”—“ellipse shape”—“petal shape” under different stress conditions and in-situ stress deflection angles. In terms of scope, the plastic zone expands unevenly to the deep part of the surrounding rock with the increase in buried depth and mining-induced stress.
- (2) The unsymmetrical failure mechanism of roadway under non-orthogonal stress state was revealed. We found that the equivalent lateral pressure coefficient defined in this study determines the shape of the plastic zone. The in-situ stress deflection angle and mining-induced stress change the value of the equivalent lateral pressure coefficient, thus causing the morphology of the plastic zone to evolve. The theoretical results are studied by numerical simulation, and the evolution law of the roadway plastic zone under the same parameters was analysed. The results show that the development law of the roadway plastic zone in numerical simulation is the same as that in theoretical calculation. The comparison results verify the correctness of the theoretical calculation and numerical simulation.
- (3) The general morphology of the roadway plastic zone under different in-situ stress deflection angle, different in-situ stress magnitudes, and different mining-induced stress are given, which covers majority of the possible geological conditions. For any type of engineering cases, the corresponding shape of the plastic zone can

Fig. 21 Unsymmetrical deformation and failure of 1305 bottom drainage roadway

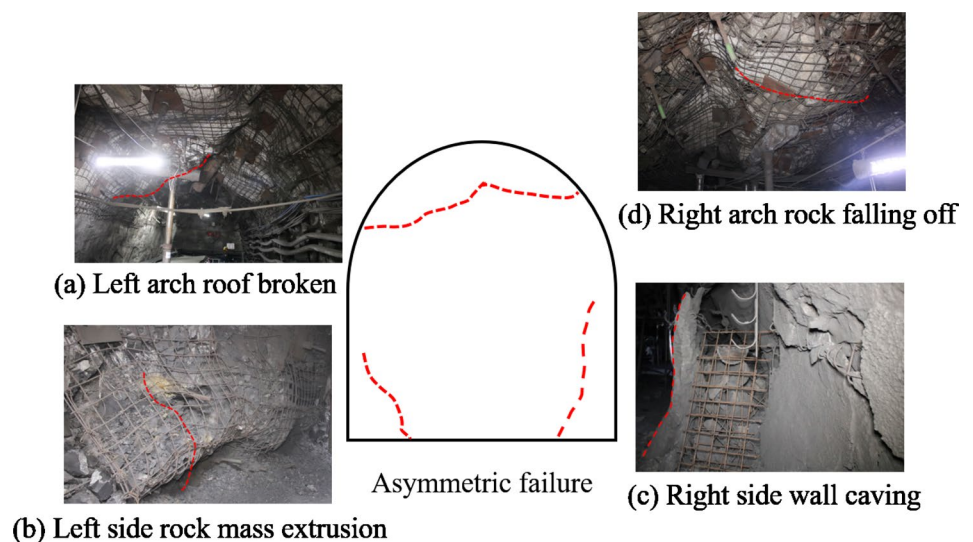
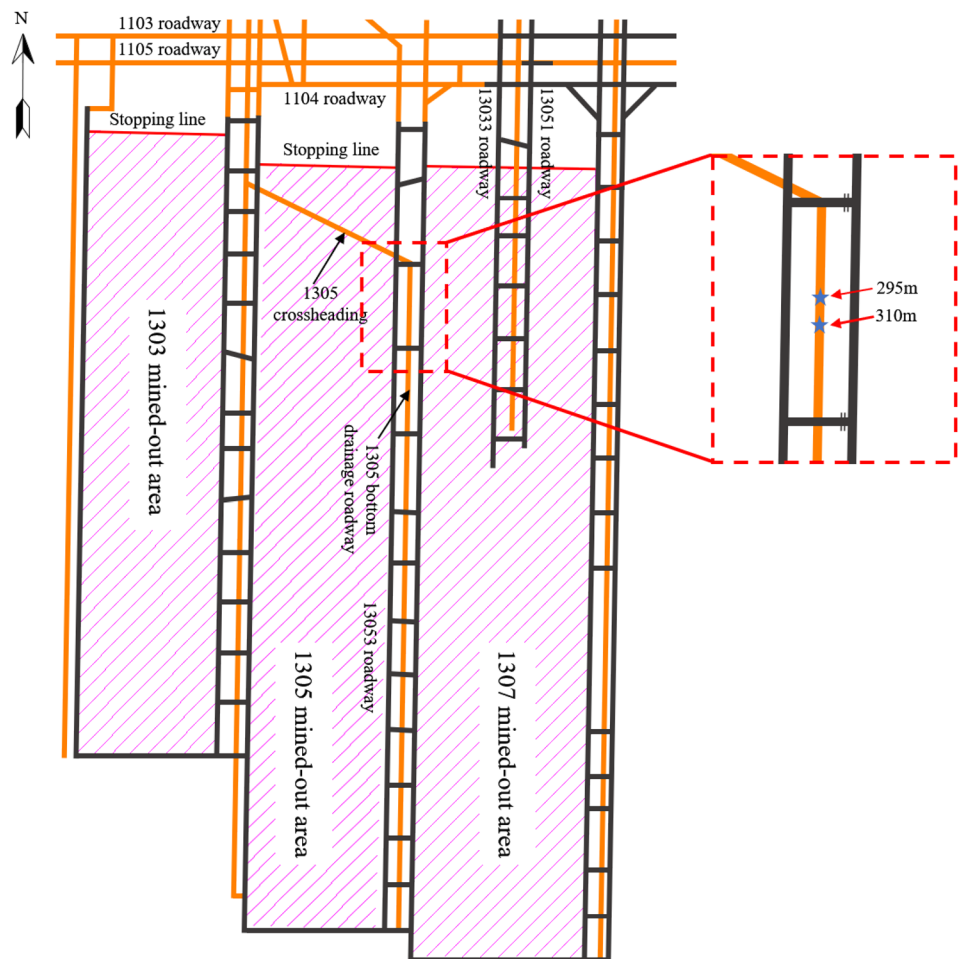


Fig. 22 Roadway layout and loose circle test points



be found in this study. Therefore, the research results of this study are extensive and universal.

- (4) Combined with field engineering examples, the calculation method in this study was verified from the perspectives of roadway failure area and loose circle depth. The failure area of the roadway is consistent with the shape of the plastic zone. The ratio of the loosening circle depth to plastic zone depth is within a fixed range. This shows that the theoretical calculation method of the roadway plastic zone in the non-orthogonal state of in-situ stress and mining-induced stress is scientific and feasible in the field.

Table 5 Comparison between field test results of loose circle in 1305 bottom pumping roadway and theoretical results of plastic zone

Measuring point (m)	Number	Loose circle results (m)	Plastic zone results	Ratio of loose circle to plastic zone
295	1#	1.1	1.62	0.679
	2#	1.2	1.85	0.648
310	1#	1.0	1.64	0.609
	2#	1.3	1.86	0.698

The failure of roadway is a very complex process. There are multiple factors that can affect the final failure modes. Factors such as rock heterogeneity and mining methods can have a certain impact on the failure modes. In this study, a certain assumption was adopted, namely that the rock mass is homogeneous and does not have a layered structure. Based on this assumption, this paper considers two main stress factors, in-situ stress and mining-induced stress, which lead to the mechanism of roadway failure. In future research, further

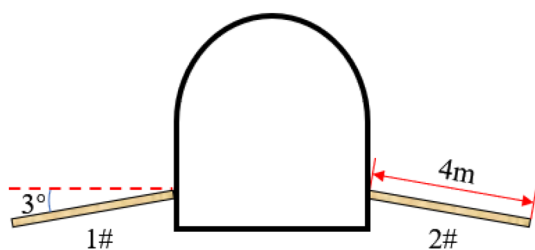
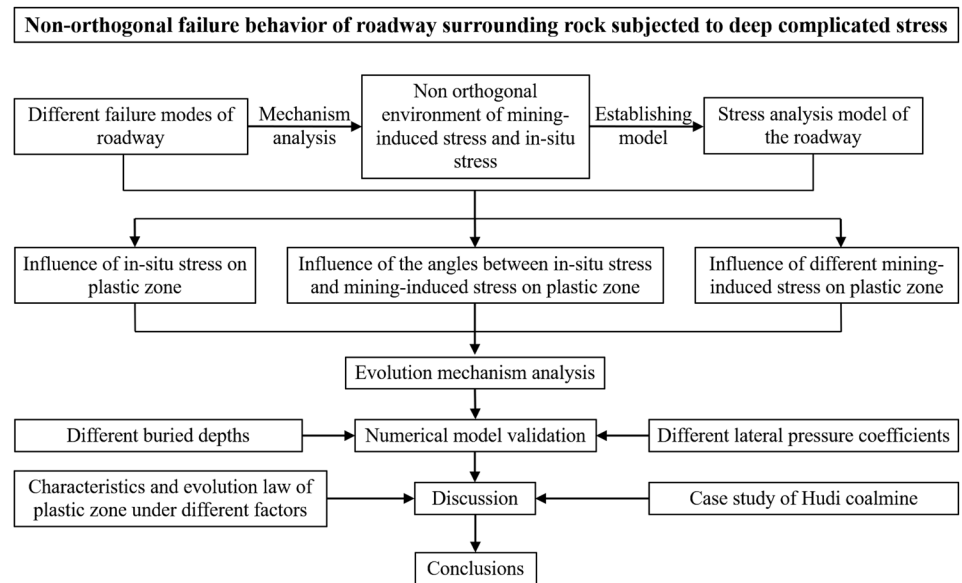


Fig. 23 Layout of loose circle test boreholes

Fig. 24 Research flowchart



consideration will be given to the heterogeneity of the rock mass, changes in mining methods, and three-dimensional stress conditions.

Acknowledgements This work was financially supported by the projects (Grants No: 52225404) supported by NSFC, Beijing Outstanding Young Scientist Program (BJJWZYJH01201911413037) and the Fundamental Research Fund of the Central Universities of China (2022YJSLJ02).

Funding NSFC, 52225404, Jianping Zuo; Beijing Outstanding Young Scientist Program, BJJWZYJH01201911413037, Jianping Zuo; Fundamental Research Fund of the Central Universities of China, 2022YJSLJ02, Jianping Zuo.

Data availability statement The data used to support the findings of this study are available from the corresponding author upon request.

Declarations

Conflict of Interest The authors declare that there are no conflicts of interest regarding the publication of this paper.

References

- Aydin G (2015) The application of trend analysis for coal demand modeling. *Eng Source Part B* 10(2):183–191. <https://doi.org/10.1080/15567249.2013.813611>
- Aydin G, Kaya S, Karakurt I (2015) Modeling of coal consumption in Turkey: an application of trend analysis. In: 24th International Mining Congress and Exhibition of Turkey, Antalya, Turkey. 2015:83–87
- British Petroleum (2022) BP statistical review of world energy. London
- Brown L, Hudyma M (2017) Identifying local stress increase using a relative apparent stress ratio for populations of mining-induced seismic events. *Can Geotech J* 54(1):128–137. <https://doi.org/10.1139/cgj-2016-0050>
- Brown ET, Bray JW, Ladanyi B et al (1983) Ground response curves for rock tunnels. *J Geotech Eng* 109(1):15–39. [https://doi.org/10.1061/\(ASCE\)0733-9410\(1983\)109:1\(15\)](https://doi.org/10.1061/(ASCE)0733-9410(1983)109:1(15))
- Caquot A (1940) Le recordement parfait. *Revue Générale des-Chemins de Fer*
- Fan L, Wang WJ, Yuan C et al (2020) Research on large deformation mechanism of deep roadway with dynamic pressure. *Energy Sci Eng* 8(9):3348–3364. <https://doi.org/10.1002/ese3.672>
- Feng G, Wang XC, Wang M et al (2020) Experimental investigation of thermal cycling effect on fracture characteristics of granite in a geothermal-energy reservoir. *Eng Fract Mech* 235:107180. <https://doi.org/10.1016/j.engfracmech.2020.107180>
- Fenner R (1938) *Untersuchungen zurerkenntnis des gebirgsdrucks*. Glückauf
- Fujii Y, Ishijima Y, Ichihara Y et al (2011) Mechanical properties of abandoned and closed roadways in the Kushiro Coal Mine, Japan. *Int J Rock Mech Min* 48(4):585–596. <https://doi.org/10.1016/j.ijrmm.2011.04.012>
- Guo XF, Zhao ZQ, Gao X et al (2019) Analytical solutions for characteristic radii of circular roadway surrounding rock plastic zone and their application. *Int J Min Sci Techno* 29(2):263–272. <https://doi.org/10.1016/j.ijmst.2018.10.002>
- Guo XF, Li C, Huo TL (2021) A quantitative evaluation method on the stability of roadway surrounding rock in partial confining stress based on plastic zone shapes. *Geomech Eng* 25(5):405–415. <https://doi.org/10.12989/gae.2021.25.5.405>
- Herrera C, Cassidy JF, Dosso SE et al (2021) The crustal stress field inferred from focal mechanisms in northern Chile. *Geophys Res Lett* 48(8):e2021GL092889. <https://doi.org/10.1029/2021GL092889>
- Kang H, Zhang X, Si L et al (2010) In-situ stress measurements and stress distribution characteristics in underground coal mines in China. *Eng Geol* 116(3–4):333–345. <https://doi.org/10.1016/j.enggeo.2010.09.015>
- Kastner H (1962) *Statik des tunnel- und stollenbaues*. Springer, Berlin
- Kodama J, Miyamoto T, Kawasaki S et al (2013) Estimation of regional stress state and Young's modulus by back analysis of mining-induced deformation. *Int J Rock Mech Min* 63:1–11. <https://doi.org/10.1016/j.ijrmm.2013.05.007>

- Jiang LS, Zhang PP, Chen LJ et al (2017) Numerical approach for goaf-side entry layout and yield pillar design in fractured ground conditions. *Rock Mech Rock Eng* 50(11):3049–3071. <https://doi.org/10.1007/s00603-017-1277-0>
- Li SW, Gao MZ, Yang XJ et al (2018) Numerical simulation of spatial distributions of mining-induced stress and fracture fields for three coal mining layouts. *J Rock Mech Geotech* 10(5):907–913. <https://doi.org/10.1016/j.jrmge.2018.02.008>
- Li G, Ma FS, Guo J et al (2020) Study on deformation failure mechanism and support technology of deep soft rock roadway. *Eng Geol* 264:105262. <https://doi.org/10.1016/j.enggeo.2019.105262>
- Lin C, Zou DHS (2021) Formulation and verification of 3D in-situ stress estimation based on differential-direction drilling. *Int J Rock Mech Min* 145:104833. <https://doi.org/10.1016/j.ijrmmms.2021.104833>
- Lucianetti G, Cianfarra P, Mazza R (2017) Lineament domain analysis to infer groundwater flow paths: clues from the Pale di San Martino fractured aquifer, Eastern Italian Alps. *Geosphere* 13(5):1729–1746. <https://doi.org/10.1130/GES01500.1>
- Mo S, Sheffield P, Corbett P et al (2020) A numerical investigation into floor buckling mechanisms in underground coal mine roadways. *Tunn Undergr Sp Tech* 103:103497. <https://doi.org/10.1016/j.tust.2020.103497>
- Mousavipour F, Riahi MA, Moghanloo GH (2020) Prediction of in situ stresses, mud window and overpressure zone using well logs in South Pars field. *J Pet Explor Prod Te* 10(5):1869–1879. <https://doi.org/10.1007/s13202-020-00890-9>
- Papanastasiou P, Durban D (1997) Elastoplastic analysis of cylindrical cavity problems in geomaterials. *Int J Numer Anal Met* 21(2):133–149. [https://doi.org/10.1002/\(SICI\)1096-9853\(199702\)21:2%3c133::AID-NAG866%3e3.0.CO;2-A](https://doi.org/10.1002/(SICI)1096-9853(199702)21:2%3c133::AID-NAG866%3e3.0.CO;2-A)
- Paul S, Chatterjee R (2011) Determination of in-situ stress direction from cleat orientation mapping for coal bed methane exploration in south-eastern part of Jharia coalfield, India. *Int J Coal Geol* 87(2):87–96. <https://doi.org/10.1016/j.coal.2011.05.003>
- Piotr M, Łukasz O, Piotr B (2017) Modelling the small throw fault effect on the stability of a mining roadway and its verification by in situ investigation. *Energies* 10(12):2082. <https://doi.org/10.3390/en10122082>
- Rajabi M, Sherkati S, Bohloli B et al (2010) Subsurface fracture analysis and determination of in-situ stress direction using FMI logs: an example from the Santonian carbonates (Ilam formation) in the Abadan Plain, Iran. *Tectonophysics* 492(1–4):192–200. <https://doi.org/10.1016/j.tecto.2010.06.014>
- Rezaei M, Hossaini MF, Majidi A (2015) Determination of longwall mining-induced stress using the strain energy method. *Rock Mech Rock Eng* 48(6):2421–2433. <https://doi.org/10.1007/s00603-014-0704-8>
- Roussev P (1998) Calculation of the displacements and Pacher's rock pressure curve by the associative law for the fluidity-plastic flow. *Tunn Undergr Sp Tech* 13(4):441–451. [https://doi.org/10.1016/S0886-7798\(98\)00087-X](https://doi.org/10.1016/S0886-7798(98)00087-X)
- Singh AK, Singh R, Maiti J et al (2011) Assessment of mining induced stress development over coal pillars during depillaring. *Int J Rock Mech Min* 48(5):805–818. <https://doi.org/10.1016/j.ijrmmms.2011.04.004>
- Song HQ, Zuo JP, Liu HY et al (2021) The strength characteristics and progressive failure mechanism of soft rock-coal combination samples with consideration given to interface effects. *Int J Rock Mech Min* 138:104593. <https://doi.org/10.1016/j.ijrmmms.2020.104593>
- Sun YJ, Zuo JP, Karakus M et al (2021) A new theoretical method to predict strata movement and surface subsidence due to inclined coal seam mining. *Rock Mech Rock Eng* 54(6):2723–2740. <https://doi.org/10.1007/s00603-021-02424-z>
- Talobre J (1960) *Rock mechanics*. Paris: Dunod
- Wang GF, Gong SY, Dou LM et al (2019) Behaviour and bursting failure of roadways based on a pendulum impact test facility. *Tunn Undergr Sp Tech* 92:103042. <https://doi.org/10.1016/j.tust.2019.103042>
- Xu SQ, Yu MH (2006) The effect of the intermediate principal stress on the ground response of circular openings in rock mass. *Rock Mech Rock Eng* 39(2):169–181. <https://doi.org/10.1007/s00603-005-0064-5>
- Yamamoto K (2009) A theory of rock core-based methods for in-situ stress measurement. *Earth Planets Space* 61(10):1143–1161. <https://doi.org/10.1186/BF03352966>
- Yang SQ, Chen M, Jing HW et al (2017) A case study on large deformation failure mechanism of deep soft rock roadway in Xin'An coal mine. *China Eng Geol* 217:89–101. <https://doi.org/10.1016/j.enggeo.2016.12.012>
- Yu H, Niu ZY, Kong LG et al (2015a) Mechanism and technology study of collaborative support with long and short bolts in large-deformation roadways. *Int J Min Sci Techno* 25(4):587–593. <https://doi.org/10.1016/j.ijmst.2015.05.011>
- Yu WJ, Wang WJ, Chen XY et al (2015b) Field investigations of high stress soft surrounding rocks and deformation control. *J Rock Mech Geotech* 7(4):421–433. <https://doi.org/10.1016/j.jrmge.2015.03.014>
- Yu ML, Zuo JP, Sun YJ et al (2022) Investigation on fracture models and ground pressure distribution of thick hard rock strata including weak interlayer. *Int J Min Sci Techno* 32(1):137–153. <https://doi.org/10.1016/j.ijmst.2021.10.009>
- Zhang AL, Xie HP, Zhang R et al (2023) Mechanical properties and energy characteristics of coal at different depths under cyclic triaxial loading and unloading. *Int J Rock Mech Min* 161:105271. <https://doi.org/10.1016/j.ijrmmms.2022.105271>
- Zhou QL, Cao P, Huang LQ (2020) A 2-D differential-stress-based analysis on the tendency of mining-induced fault reactivation. *Environ Earth Sci* 79:1–11. <https://doi.org/10.1007/s12665-020-09033-z>
- Zuo JP, Peng SP, Li YJ et al (2009) Investigation of karst collapse based on 3-D seismic technique and DDA method at Xieqiao coal mine, China. *Int J Coal Geol* 78(4):276–287. <https://doi.org/10.1016/j.coal.2009.02.003>
- Zuo JP, Wen JH, Li YD et al (2019) Investigation on the interaction mechanism and failure behavior between bolt and rock-like mass. *Tunn Undergr Sp Tech* 93:103070. <https://doi.org/10.1016/j.tust.2019.103070>
- Zuo JP, Liu HY, Liu DJ et al (2021) Study on large deformation mechanism and concrete-filled steel tubular support technology for ventilation shaft roadway. *B Eng Geol Environ* 80:6245–6262. <https://doi.org/10.1007/s10064-021-02331-1>

Publisher's Note Springer Nature remains neutral with regard to jurisdictional claims in published maps and institutional affiliations.

Springer Nature or its licensor (e.g. a society or other partner) holds exclusive rights to this article under a publishing agreement with the author(s) or other rightsholder(s); author self-archiving of the accepted manuscript version of this article is solely governed by the terms of such publishing agreement and applicable law.